© 2019. Published by The Company of Biologists Ltd | Development (2019) 146, dev177105. doi:10.1242/dev.177105

RESEARCH ARTICLE

Organ-specific genetic interactions between paralogues of the *PXY* and *ER* receptor kinases enforce radial patterning in *Arabidopsis* vascular tissue

Ning Wang[1,2,*,¶], Kristine S. Bagdassarian[1,¶], Rebecca E. Doherty[1,‡,¶], Johannes T. Kroon[1], Katherine A. Connor[1], Xiao Y. Wang[3,§], Wei Wang[2], Ian H. Jermyn[4], Simon R. Turner[3] and J. Peter Etchells[1,]**

ABSTRACT

In plants, cells do not migrate. Tissues are frequently arranged in concentric rings; thus, expansion of inner layers is coordinated with cell division and/or expansion of cells in outer layers. In *Arabidopsis* stems, receptor kinases, *PXY* and *ER*, genetically interact to coordinate vascular proliferation and organisation via inter-tissue signalling. The contribution of *PXY* and *ER* paralogues to stem patterning is not known, nor is their function understood in hypocotyls, which undergo considerable radial expansion. Here, we show that removal of all *PXY* and *ER* gene-family members results in profound cell division and organisation defects. In hypocotyls, these plants failed to transition to true radial growth. Gene expression analysis suggested that *PXY* and *ER* cross- and inter-family transcriptional regulation occurs, but it differs between stem and hypocotyl. Thus, *PXY* and *ER* signalling interact to coordinate development in a distinct manner in different organs. We anticipate that such specialised local regulatory relationships, where tissue growth is controlled via signals moving across tissue layers, may coordinate tissue layer expansion throughout the plant body.

KEY WORDS: *Arabidopsis*, Cambium, Phloem, Procambium, Signalling, Xylem

INTRODUCTION

Cell migration is fundamental to the development of animal body plans. By contrast, plant cell walls do not allow cells to migrate, and consequently plant growth and development is entirely a result of differential growth. As such, initiation and elaboration of plant organs occurs via coordinated changes to the orientation and occurrence of cell divisions, and by cell expansion. In *Arabidopsis* embryos, pattern is established early in development. Twenty-eight-cell embryos have already specified the provascular tissue that consists of four cells the centre of the embryo. A layer of endodermal tissue surrounds the provasculature, and an outer layer of epidermal cells has also been specified (ten Hove et al., 2015). Extra tissue types, cortex and pericycle, are subsequently derived from specific rounds of asymmetric cell division (Kajala et al., 2014). In the hypocotyl, the vascular tissue undergoes a transition from diarch to radial symmetry 6-10 days post-germination. Here, cells adjacent to the xylem divide to generate the vascular cambium (Smetana et al., 2019), such that the tissue pattern along the radial axis becomes epidermis-cortex-endodermis-pericycle-phloem-cambium-xylem. As the hypocotyl further expands, the epidermis and cortex are lost in a process that corresponds with periderm specification and proliferation at around 3 weeks post-germination (Wunderling et al., 2018). Thus, a morphology periderm-phloem-cambium-xylem is generated and maintained through the remainder of life of the plant (Chaffey et al., 2002).

Coordination of tissue expansion must occur as the hypocotyl transitions from diarch to radial symmetry, and as organs increase in size. This coordination must incorporate cell division, because cell numbers increase from tens to hundreds to thousands of cells. It must also incorporate cell size, which differs according to cellular function in differentiated cells. Consequently, the *Arabidopsis* hypocotyl represents an interesting model for studying how patterns are maintained through very large increases in plant size, a mechanism that is poorly understood. This organisation contrasts with that of the *Arabidopsis* inflorescence stem, where radial growth is much more limited. Here, radial pattern is defined in the rib zone below the shoot apex, rather than built upon a pre-existing embryonic pattern. The tissue types along the radial axis of the stem also differ. Epidermis, cortex and endodermis are present outside the phloem, procambium and xylem (Fig. 1A). Pith constitutes the cell type at the centre of the stem.

Evidence points to the presence of mechanisms that coordinate the order of tissue layers. In the *Arabidopsis* root, removal of the root tip results in a reorganisation of the organ to enable the formation of a new meristem. Strikingly, stable patterning of tissue layers is established in the reorganised tissue separately from the activity of the stem cell niche. This suggests that tissue layer organisation is independent of stem cell growth (Efroni et al., 2016). Non-cell autonomous signalling represents one mechanism through which tissue layer organisation could be coordinated. A ligand secreted by one tissue could provide positional information to a receptor located in an adjacent cell type. Ligand-receptor pairs that signal between tissue layers and are required for tissue layer organisation have been described. TRACHEARY ELEMENT DIFFERENTIATION INHIBITORY FACTOR (TDIF) is a ligand that is encoded for by three genes, *CLAVATA3-LIKE/ESR-RELATED 41* (*CLE41*), *CLE42* and *CLE44*. TDIF is excreted from the phloem and perceived by a receptor kinase, PHLOEM

[1]Department of Biosciences, Durham University, South Road, Durham, DH1 3LE, UK. [2]College of Life Science, Henan Agricultural University, 95 Wenhua Road, Zhengzhou 450002, China. [3]Faculty of Biology, Medicine & Health, University of Manchester, Manchester M13 9PT, UK. [4]Department of Mathematical Sciences, Durham University, South Road, Durham DH1 3LE, UK.
*Present address: School of Life Science, Beijing Institute of Technology, 5 South Zhongguancun Street, Haidian District, Beijing 100081, People's Republic of China. ‡Present address: The John Innes Centre, Colney Lane, Norwich NR4 7UH, UK. §Present address: Department of Plant Sciences, University of Cambridge, Downing Street, Cambridge CB2 3EA, UK.
¶These authors contributed equally to this work.

**Author for correspondence (peter.etchells@durham.ac.uk)

W.W., 0000-0002-3711-5181; J.P.E., 0000-0002-8524-4949

Received 19 February 2019; Accepted 23 April 2019

Development (2019) 146, dev177105. doi:10.1242/dev.177105

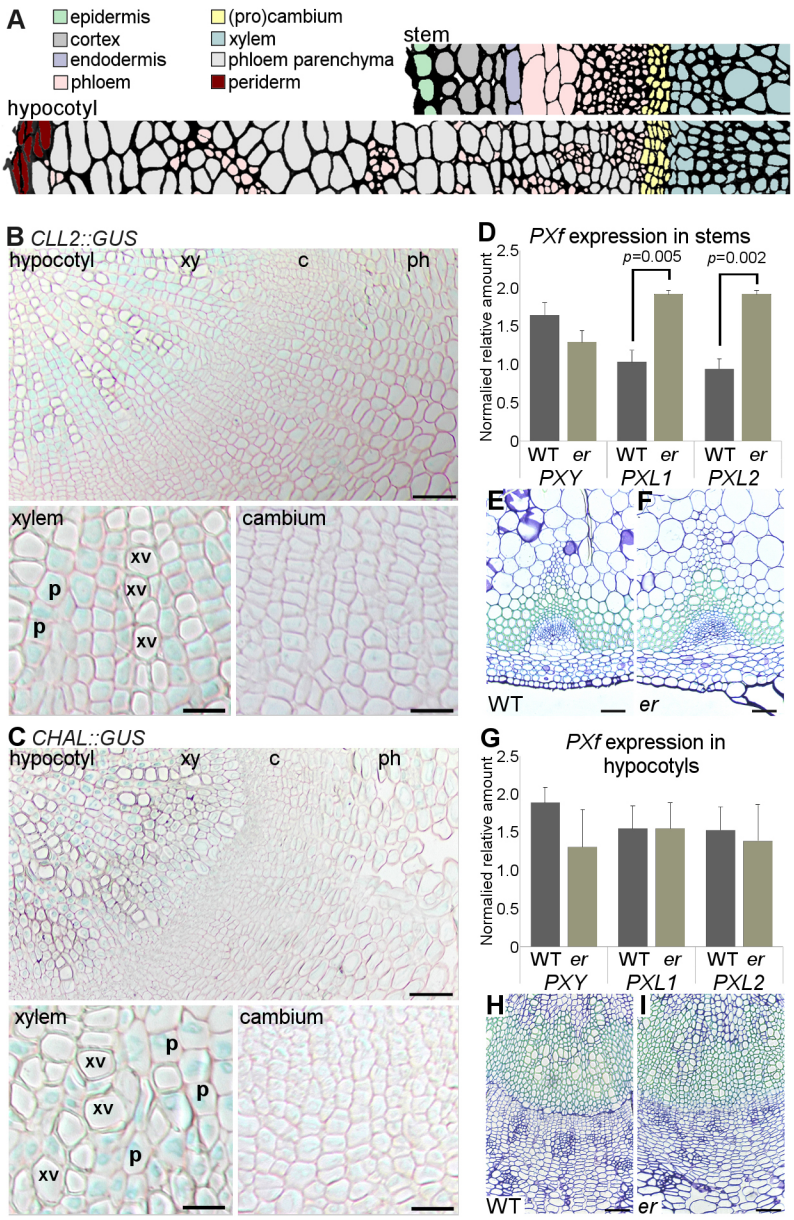

Fig. 1. Analysis of *CLL2*, *CHAL*, *PXL1* and *PXL2* expression. (A) Tissue types in the *Arabidopsis* stem and hypocotyl. (B,C) Spatial expression of *CLL2* (B) and *CHAL* (C) in hypocotyl transverse sections determined using *GUS* transcriptional fusions. (D) Graph showing qRT-PCR results for expression of *PXL1* and *PXL2* normalised to *ACT2* in wild-type and *er* mutant inflorescence stems from 5-week-old plants. (E,F) Wild-type (E) and *er* (F) stem vascular bundles. (G) Graph showing qRT-PCR results for expression of *PXY*, *PXL1* and *PXL2* normalised to *ACT2* in wild-type and *er* mutant hypocotyls at 5 weeks of age. (H,I) Transverse sections of wild-type (H) and *er* (I) hypocotyls. In qRT-PCRs (D,G), *P* values were calculated using Student's *t*-test. Scale bars: 50 µm in B,C (upper), E,F,H,I; 20 µm in B,C (lower). xy, xylem; c, cambium; ph, phloem; p, xylem parenchyma; xv, xylem vessels.

INTERCALATED WITH XYLEM (PXY), which is expressed in the cambium. Loss of TDIF-PXY results in a failure to correctly organise tissue layers in the vascular tissue. *pxy* mutants are characterised by disruption to the spatial separation of xylem, cambium and phloem. Reductions in cell division in the cambium and premature xylem differentiation are also a consequence of loss of *PXY* (Etchells and Turner, 2010; Fisher and Turner, 2007; Han et al., 2018; Hirakawa et al., 2010; Hirakawa et al., 2008; Ito et al., 2006; Kondo et al., 2014; Suer et al., 2011). TDIF-PXY signalling thus represents a mechanism through which differential growth in vascular tissue could be coordinated, regulating as it does, tissue organisation, cell division and differentiation.

TDIF-PXY genetically interacts with a second ligand-receptor pair to maintain the spatial separation of vascular tissues. In stems, the *ERECTA* (*ER*) receptor is expressed in the phloem, and its cognate ligands, *CHALLAH-LIKE 2*/*EPIDERMAL PATTERNING FACTOR-LIKE 4* (*CLL2*/*EPFL4*) and *CHALLAH* (*CHAL*/*EPFL6*) are expressed in the endodermis (Abrash et al., 2011; Uchida et al., 2012). *pxy er* mutant stems show organisation defects greater than those of *pxy* single mutants (Etchells et al., 2013). Thus, in stems, the genetic interaction between EPFL-ER and TDIF-PXY represents a non-cell autonomous signalling system that organises tissue layers between endodermis, phloem, cambium and xylem. In hypocotyls, changes to the organisation of vascular tissues in *er pxy* hypocotyls are also apparent (Etchells et al., 2013). However, *ER* expression is reported to be much broader, being present in phloem, cambium and xylem parenchyma (Ikematsu et al., 2017). The spatial expression domains of *CHAL* and *CLL* genes have not been described in hypocotyls.

In the *Arabidopsis* genome, paralogues of both *PXY* and *ER* are present. The *PXY* family, hereafter referred to as *PXf*, comprises *PXY*, *PXY-LIKE1* (*PXL1*) and *PXY-LIKE2* (*PXL2*). TDIF is reported to bind the ligand binding pocket of PXL1 and PXL2 (Zhang et al., 2016), and *pxl1* and *pxl2* enhance the vascular organisation defects that are characteristic of *pxy* mutants (Etchells et al., 2013; Fisher and Turner, 2007). The *ER* paralogues are *ER-LIKE1* (*ERL1*) and *ERL2* (Shpak et al., 2004). The *ERECTA* family (*ERf*) have wide-ranging roles in regulation of plant growth and development.

Development (2019) 146, dev177105. doi:10.1242/dev.177105

Redundantly, these three genes function in cell elongation, cell division, inflorescence architecture (Shpak et al., 2004; Torii et al., 1996), floral patterning (Bemis et al., 2013), shoot apical meristem fate (Kimura et al., 2018; Uchida et al., 2013) and stomatal spacing (Shpak et al., 2005). In the context of plant vascular development, they promote vascular expansion in the stem (Uchida and Tasaka, 2013). By contrast, in hypocotyls they repress radial expansion and also control the timing of xylem fibre formation (Ikematsu et al., 2017; Ragni et al., 2011). A hallmark of loss of *ER*f genes is an increase in cell size, particularly with respect to the radial axis (Shpak et al., 2004; Shpak et al., 2003).

In this article, we have investigated the genetic relationships between *PX*f and *ER*f receptors. We generated *pxy pxl1 pxl2 er erl1 erl2* sextuple mutants using a combination of classical genetics and genome editing. In hypocotyls, the sextuple mutant failed to make the transition to secondary growth. Further analysis of these lines demonstrated that *PX*f and *ER*f genetically interact to coordinate tissue integrity at the levels of both cell size and cell division. Gene expression analysis in stems and hypocotyls suggested that members of *PXY* and *ER* gene families regulated expression of paralogues both within and between these families. However, this regulation was distinct in hypocotyls and stems. In stems, *PX*f and *ER* also influenced the expression of non-vascular-expressed *EPFL4* and *EPFL6*. This suggests that coordination of growth regulators occurs between vascular and non-vascular tissue layers. Our results demonstrate that although interactions between members of both families are crucial in both stem and hypocotyl, the paralogues have specialised functions within vascular tissue of differing ontogenies.

RESULTS

PXL1 and *PXL2* expression is elevated in *er* stems.

In *Arabidopsis* stems and hypocotyls, tissue is arranged in concentric rings with the vasculature at the centre (Fig. 1A). *PXY* and *ER* genetically interact to control vascular development. In stems, ER ligands, CHAL and CLL2 (Abrash et al., 2011), are expressed in the endodermis whereas *ER* is expressed in the phloem (Uchida et al., 2012). TDIF-encoding genes are expressed in the phloem, and TDIF signals to PXY, which is expressed in the procambium (Etchells and Turner, 2010; Fisher and Turner, 2007; Hirakawa et al., 2008). In mature hypocotyls, endodermis is not present and the *CLL2* and *CHAL* domains of expression are not known. To better understand the spatial relationships between the PXY and ER receptors and ER ligands in hypocotyls, we determined the *CHAL* and *CLL2* expression pattern in 5-week-old plants using transcriptional reporters (Abrash et al., 2011). Both *CHAL::GUS* and *CLL2::GUS* lines demonstrated clear expression maxima both in xylem parenchyma and in the differentiating xylem adjacent to the cambium (Fig. 1B,C). Expression in the cambium itself was minimal. Thus, active ER ligand-receptor complexes occur in different locations in stems compared with hypocotyls. In stem tissue, active ER ligand-receptor complexes would be in the phloem, whereas in hypocotyls they must predominate in differentiating xylem.

To better understand the influence that *ER* might have upon PXY signalling, we tested whether expression levels of genes involved in PXY signalling differed in *er* mutants. We have previously shown that TDIF-encoding *CLE41*, *CLE42* and *CLE44* levels are unchanged in *er* (Etchells et al., 2013), so we analysed expression of the *PX*f family of receptors. qRT-PCR was used to test levels of *PX*f gene expression in stems and hypocotyls of 5-week-old wild-type and *er* plants (Fig. 1D-I). In hypocotyls, the level of *PX*f gene expression was unchanged in *er* mutants compared with wild type (Fig. 1G). By contrast, *PXL1* and *PXL2* expression, but not that of *PXY* was found to be elevated in *er* mutant stems (Fig. 1D). These observations suggest that *ER* signalling may regulate vascular development by setting *PXL1* and *PXL2* levels in the stem. They also underline that there are differences in regulatory relationships between patterning genes in stem and hypocotyl.

Genetic interactions between *ER* and *PX*f in stems and hypocotyls

We sought to further investigate the role of *PXL1* and *PXL* in vascular development. In transverse sections, *pxl1 pxl2* double mutants were indistinguishable from wild type (Fig. S1); however, we have previously shown that *pxl1* and *pxl2* enhance the *pxy* phenotype (Etchells et al., 2013; Fisher and Turner, 2007) (Figs 2A,B and 3D). Thus, as *PXL* gene expression was observed to be elevated in *er* stems, but neither *er* (Fig. 1E-F) nor *pxl1 pxl2* (Fig. S1) lines had vascular stem phenotypes except in a *pxy* mutant background, we addressed the function of *PXL1* and *PXL2* regulation by *ER* in the absence of *pxy*. *er px*f quadruple mutants (*er pxy pxl1 pxl2*) were generated and compared with wild-type, *pxy*, *er*, *er pxy* and *px*f lines. In inflorescence stems, *er px*f lines had considerably fewer cells per vascular bundle than either *px*f, *er* or *pxy er* counterparts (Fig. 2A; Tables S1 and S2). Therefore *PXL1* and *PXL2* do function redundantly with *ER* to regulate vascular proliferation in the stem, at least in the absence of *PXY*. In hypocotyls, a reduction in radial growth was observed in *px*f *er* lines relative to *px*f and *er*; however, *px*f *er* and *pxy er* lines were indistinguishable (Fig. 3; Tables S1 and S3). Thus, *pxl1* and *pxl2* do not enhance *pxy er* hypocotyl phenotypes, a result consistent with our observation that *PXL1* and *PXL2* expression was unchanged in *er* mutant hypocotyls (Fig. 1G).

Although changes to vascular proliferation were apparent in *er px*f inflorescence stems, by far the most dramatic defect was observed when the vascular bundle shape was assessed (Fig. 2B-F). In wild-type *Arabidopsis* stems, the distribution of vascular bundles is such that there is a greater distribution of vascular tissue along radial axis of the stem than along the tangential (Fig. 2C). We found the tangential:radial length ratio of wild-type vascular bundles to be 0.61. In *px*f and *pxy er* lines, this ratio was 0.91 and 1.36, respectively. In *er px*f stems, a dramatic redistribution of vascular cell types had occurred along the tangential axis (Fig. 2F), such that the ratio of tangential:radial length of vascular tissue was 2.30 (Fig. 2B; Table S1). In some plant stems, this led to an almost complete ring of vascular tissue, with phloem cells scattered around the circumference of the vascular cylinder (arrows in Fig. 2F), rather than present in discrete vascular bundles (Fig. 2C,D). Thus, *PXL1* and *PXL2* are crucial for regulating radial pattern in the stem, particularly in the absence of *ER* and *PXY*, and these data support the idea that *ER* and *PX*f constitute a mechanism for organising vascular cell layers.

Stem *ER*f expression is subject to the presence of *ER* and *PX*f.

Having observed that *PX*f genes were differentially expressed in *er* mutants (Fig. 1D), and that *PXL1* and *PXL2* contribute to the control of stem radial pattern (Fig. 2), we also sought to determine whether expression of members of the *ER* gene family were changed in response to perturbation of *PX*f or *ER* genes. In stems and hypocotyls of *px*f lines, *ER* expression did not differ from wild-type levels, as determined by qRT-PCR. Expression levels of *ERL1* and *ERL2* were also indistinguishable in wild-type, *er* and *px*f stems (Fig. 4A-C). By contrast, *ERL1* expression was significantly reduced when *er px*f lines were compared with *er* single mutants.

Development (2019) 146, dev177105. doi:10.1242/dev.177105

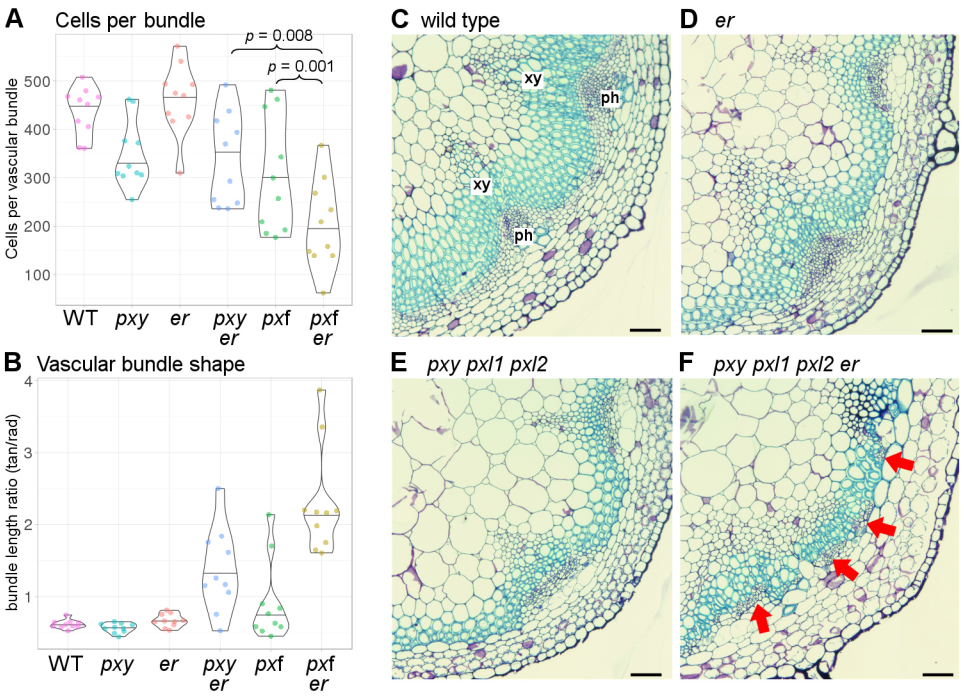

Fig. 2. Comparison of vascular tissue in stems of *pxf er* lines and controls. (A) Violin plot showing mean cells per vascular bundle. (B) Violin plot showing representation of vascular bundle arrangement (bundle tangential/radial axes ratio). (C-F) Transverse sections through wild-type (C), *er* (D), *pxf* (E) and *pxf er* (G) stems. Arrows in F indicate phloem distributed around the stem, rather than in discrete bundles, as seen in other genotypes (C-E). *P* values were calculated using ANOVA with an LSD post-hoc test (A). Scales bars: 50 µm. xy, xylem; ph, phloem.

Thus *ERL1* expression in *er* mutants is maintained by the *PXF* in stems (Fig. 4A). Expression levels of the ER ligands that function in the stem, *CHAL* and *CLL2*, were also tested in this experiment, as was that of *CLL1*, which genetically interacts *CHAL* and *CLL2* (Abrash et al., 2011; Uchida et al., 2012; Uchida and Tasaka, 2013). Inflorescence stem expression of *CHAL* and *CLL2*, but not that of *CLL1*, demonstrated significant reductions in expression in *er pxf* lines when compared with *er* (Fig. 4D-F). Thus, *PXF* and *ER* genetically interact to maintain *EPFL* ligand expression in stems in addition to that of their cognate receptor, *ERL1* (Fig. 4A).

Co-regulation of *ERf* expression by *ER* and *PXF* in hypocotyls

In hypocotyls, *ERL1* acts redundantly with *ER* to repress hypocotyl growth and control the timing of xylem fibre differentiation (Ikematsu et al., 2017). *ERL2* has not been assigned a function in hypocotyl development as its expression has been reported as absent from hypocotyls in 9-day-old seedlings and 3-week-old plants (Ikematsu et al., 2017; Uchida et al., 2013). To understand how *PXY* and *ER* might influence *ERf* expression, *ERf:GUS* reporter constructs (Shpak et al., 2004) were crossed into *pxy* and *er* mutants. To our surprise, in 5-week-old plants, we did detect *ERL2::GUS* reporter expression in the hypocotyls of wild type, which, at this growth stage, demonstrated a very similar pattern to that observed for *ERL1* and *ER* (Fig. 5A,D,G). Thus, *ERL2* expression is a feature of late hypocotyl development. *ER*, *ERL1* and *ERL2* expression was present in most hypocotyl cell types, with two maxima; the first in the cambium and xylem initials, and the second in the periderm (Fig. 5A,D,G; arrowheads). No change in the pattern of *ERL1* or *ERL2::GUS* expression was observed in *er* mutants (Fig. 5C,F). However, the clearly defined expression maxima that were observed in *ER::GUS*, *ERL1::GUS* and *ERL2::GUS* lines in both wild type and *er* mutants, lacked definition in the absence of *PXY* (Fig. 5B,E,H). Here, for all three reporters, expression was

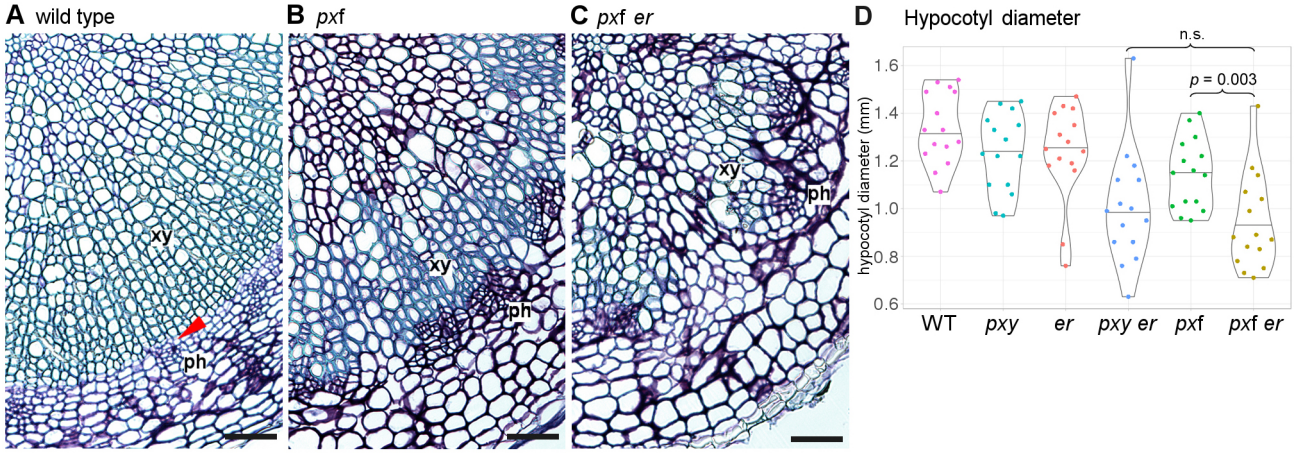

Fig. 3. Vascular tissue in hypocotyls of *pxf er* lines and controls. (A-C) Transverse sections through *Arabidopsis* hypocotyls. (A) Wild type. (B) *pxf*. (C) *pxf er*. (D) Violin plot showing reductions in hypocotyl diameter in *er pxf* lines compared with controls. Statistical significance was calculated using ANOVA plus Tukey. xy, xylem; ph, phloem. Red arrowhead in A marks dividing cambium. Scale bars: 50 µm.

Development (2019) 146, dev177105. doi:10.1242/dev.177105

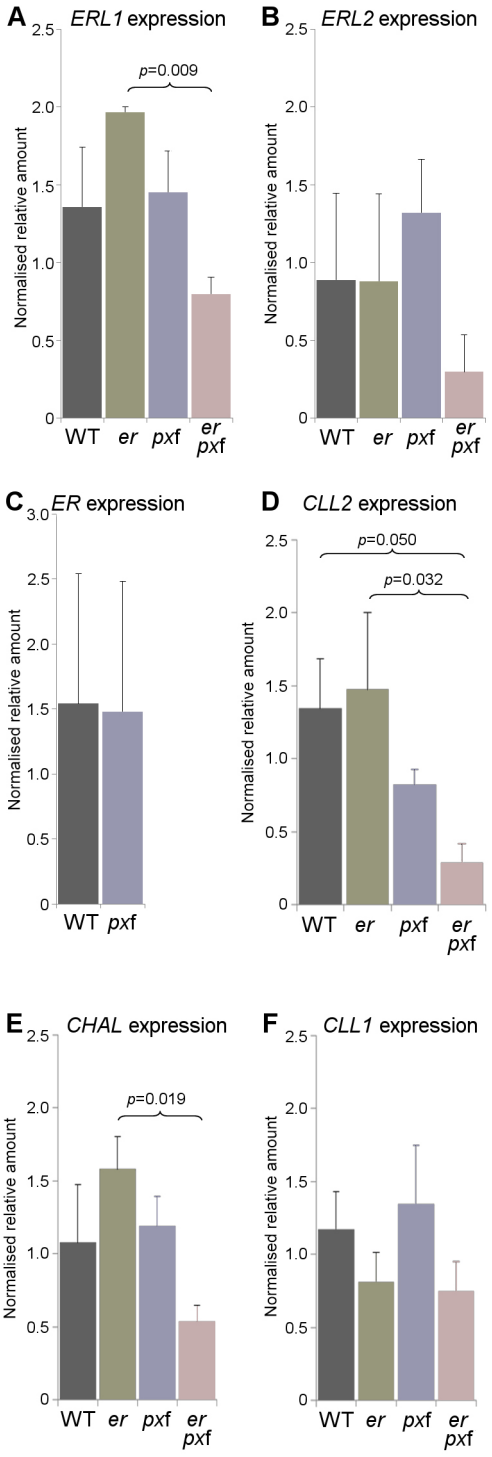

Fig. 4. qRT-PCRs showing *ER*f and *EPFL* expression in stems. (A-C) Stem expression of *ERL1* (A), *ERL2* (B) and *ER* (C) in wild type, *er*, *pxf* and *pxf er* mutants in stems. Expression was normalised to *18S* rRNA. (D-F) Expression of *CLL2* (D), *CHAL* (E) and *CLL1* (F) in hypocotyls (normalised to *18S rRNA*). *P* values were calculated using ANOVA with an LSD post-hoc test. Significant differences are marked with brackets.

observed to be more even across the hypocotyl, thus PXY signalling is either required to define *ER*f expression maxima, or cell types in which *ER*f are expressed are found throughout the hypocotyl in *pxy* mutants. The latter seems unlikely as there are fewer vascular cells in *pxy* mutants.

Having defined the pattern of *ER*f expression in a subset of genotypes, we sought to address changes to levels of *ER*f expression using qRT-PCR (Fig. 5I-K). In common with our observation in the stem (Fig. 4), hypocotyl *ERL1* and *ERL2* expression levels did not differ between wild-type, *er* and *pxf* lines (Fig. 5J-K). By contrast, a striking increase in *ERL1* and *ERL2* gene expression was observed

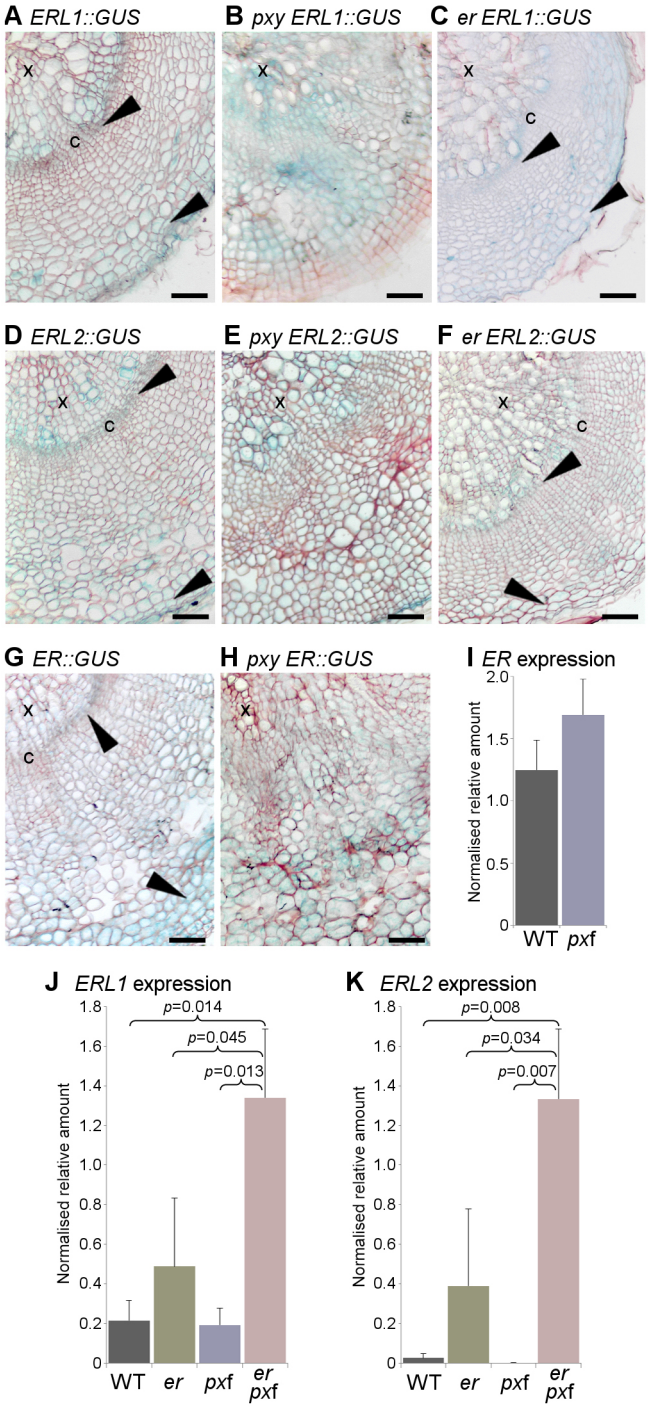

Fig. 5. *ER*f expression in hypocotyls of *pxy* and *er* lines. (A-C) *ERL1::GUS* in wild type (A), *pxy* (B) and *er* (C). (D-F) *ERL2::GUS* in wild type (D), *pxy* (E) and *er* (F). (G,H) *ER::GUS* in wild type (G) and *pxy* (H). Black arrowheads indicate expression maxima. x, xylem; c, cambium. Scale bars: 50 µm. (I-K) Expression of *ER* (I), *ERL1* (J) and *ERL2* (K) in wild-type, *er*, *pxf* and *pxf er* hypocotyls (normalised to 18S rRNA). *P* values were calculated using ANOVA and an LSD post-hoc test.

Development (2019) 146, dev177105. doi:10.1242/dev.177105

in *pxf er* hypocotyls relative to all other genotypes tested (Fig. 5J,K). As such, opposite regulation of *ERL1* and *ERL2* by *ER* and *PXf* genes occurred in the hypocotyls (Fig. 4J-K) and stem (Fig. 2A-B). This highlights a difference in the nature of the *PXf-ER* genetic interactions in stems and hypocotyls. In hypocotyls, no changes were observed in levels of *CHAL*, *CLL1* and *CLL2* expression levels in *er*, *pxf* or *er pxf* lines (Fig. S2).

Hypocotyl size and organisation in *PXf ERf* mutants

The *PXf* promotes radial growth in hypocotyls (Etchells et al., 2013; Fisher and Turner, 2007; Hirakawa et al., 2008) (Fig. 3D; Tables S1 and S3), whereas *ER* and *ERL1* signalling represses it (Ikematsu et al., 2017). Thus, our gene expression data demonstrating that *PXf* plays a part in repression of ERL gene expression in hypocotyls (Fig. 5J,K) are consistent with existing phenotypic data because the *PXf* might be expected to repress expression of negative regulators of hypocotyl radial growth. In addition to repressing radial growth, *ER* and *ERL1* have also been described as preventing premature fibre formation, as *er erl1* hypocotyls develop fibre cells in the location where parenchyma are present in wild type. *ERL2* was thought not to function in the hypocotyl given its very low expression levels in the early stages of development (Ikematsu et al., 2017). Because we found *ERL2* to be expressed in hypocotyls at 5 weeks (Fig. 5D,K), we tested whether *ERL2* functioned similarly to *ERL1* by analysing *er erl2* lines. Neither change to fibre formation, nor to hypocotyl radial growth were observed (Fig. S3); thus, in contrast to *ERL1* (Ikematsu et al., 2017), a function for *ERL2* in hypocotyl development is not apparent in a double mutant background with *er*.

To address the function of the elevated ERL gene expression that we observed in *pxf er* hypocotyls (Fig. 5J,K), we removed ERL gene function from this genotype by generating *pxf er erl1*, *pxf er erl2* and *pxf erf* quintuple and sextuple mutants. *PXY* and *ERL1* are tightly linked on chromosome 5, separated by just 270 kb, so to overcome this linkage we employed a CRISPR/cas9 construct that contained two guide RNAs against *ERL1* (Fig. S4). Thus, *pxf er erl1* and *pxf erf* plants were generated by genome editing. Secondary growth in these lines and controls was determined by measuring the hypocotyl radius in 6-week-old plants (Fig. 6A, Fig. S5C). Radii of *pxf er* and *pxf er erl1* lines did not show a significant difference. By contrast, radii of *pxf er erl2* and *pxf erf* hypocotyls were significantly smaller than those of *pxf er erl1* plants (Fig. 6A). Thus, *ERL1* and *ERL2* expression is required in *pxf er* hypocotyls to maintain hypocotyl growth rates; however, pairwise comparisons suggested that *ERL2* played a greater role than *ERL1* in this respect, as *pxf er erl1* hypocotyls were larger than those of *pxf er erl2* lines.

During vascular cylinder development in the embryo, the hypocotyl forms in a diarch pattern with a row of xylem cells that are flanked by two phloem poles (Dolan et al., 1993). As secondary growth proceeds, this organisation develops radial symmetry with phloem present around the circumference of the vascular cylinder (Chaffey et al., 2002). We analysed hypocotyl morphology in 5-week-old plants. Strikingly, development was perturbed to such a degree in *pxf erf* mutants that the position of the original phloem poles remained apparent (arrows in Fig. 6F; see Fig. S5 for higher magnification). This demonstrates that vascular development was retarded to such a degree that these plants could not make the transformation to true radial growth. Such phenotypes were not observed in *pxf*, *erf* or *pxf er erl2* lines (Fig. 6B-E).

Next, we looked to identify recent cell divisions in our mutant hypocotyls by analysing thin sections. In wild-type and *erf* lines, cell divisions were always oriented perpendicular to the hypocotyl

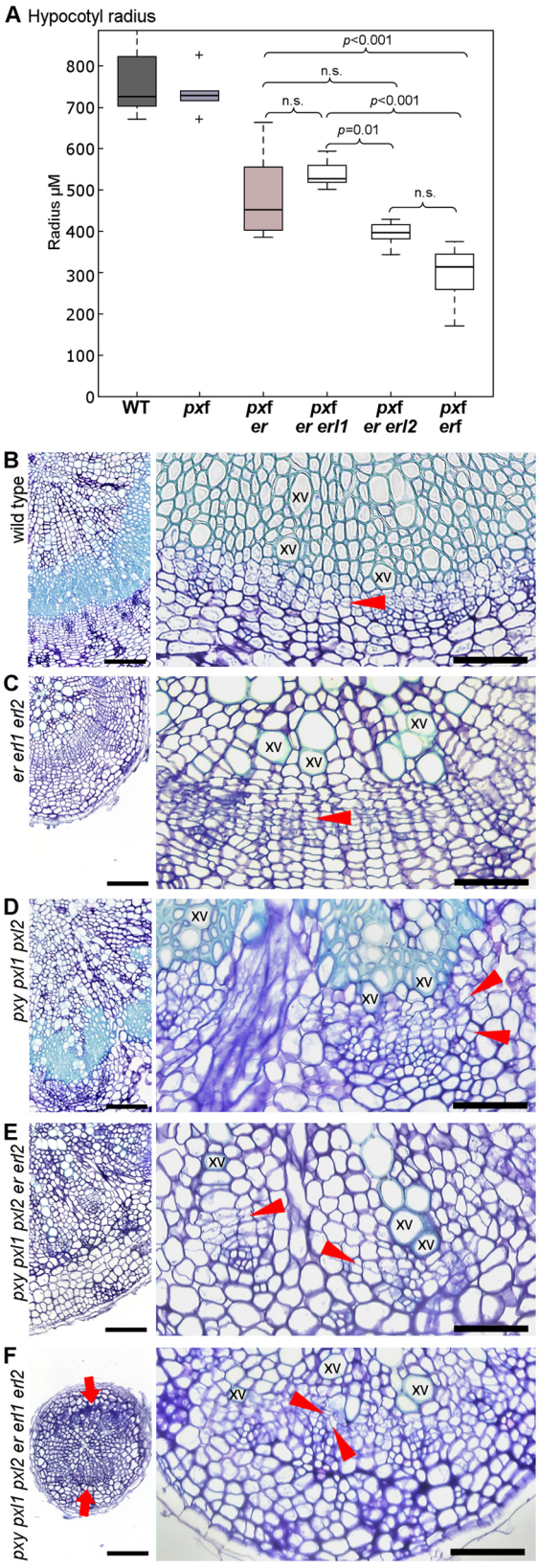

Fig. 6. Transverse sections of hypocotyls from *pxf erf* lines. (A) Boxplot showing hypocotyl radii of *pxf* lines with differing numbers of *erf* mutations. (B) Wild-type, (C) *erf*, (D) *pxf*, (E) *pxf er erl2* and (F) *pxf erf* vascular tissue. Sites of phloem poles in *pxf erf* are marked with red arrows in the left-hand panel of F (see Fig. S5 for higher magnification). Red arrowheads in B-F align with cell divisions. Scale bars: 100 µm (left); 50 µm (right); xv, xylem vessel.

Development (2019) 146, dev177105. doi:10.1242/dev.177105

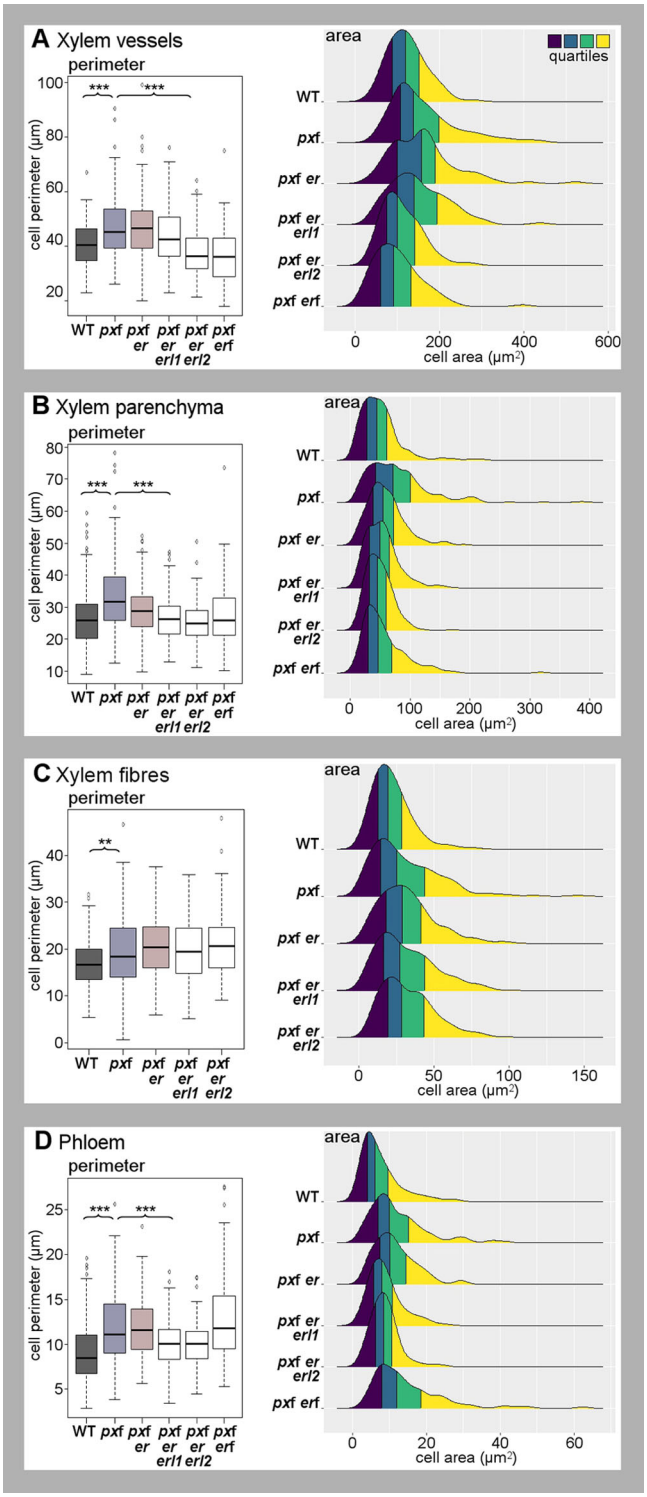

Fig. 7. Comparisons of hypocotyl cell morphology. (A-D) Boxplots on left show mean cell perimeter for xylem vessels (A), xylem parenchyma (B), fibres (C) and phloem cells (D). Boxes represent the 25th to 75th percentile, the horizontal line marks the median. Whiskers' endpoints are the min/max points within the interval spanning Q1-1.5*IQR (lower) and Q3-1.5*IQR (upper). IQR = Q3-Q1 (the length of the box). Asterisks mark significant differences (ANOVA plus Tukey; ***P<0.001, **P<0.01; see Table S4 for pairwise comparisons of P values). Ridgeline plots on the right show the distributions of cell areas divided into quartiles. Areas of *pxf* lines were greater than those of *pxf er erl2* lines in xylem vessels, phloem and parenchyma (P≤0.001) but not fibres. Differences were calculated with ANOVA and a Tukey post-hoc test; see Tables S4 and S5 for pairwise comparisons of P values.

radial axis (Fig. 6B,C, arrowheads). This aspect of normal vascular development known to perturbed in lines that lack *pxy* and its paralogues (Fig. 6D) (Fisher and Turner, 2007). Recent cell divisions were clearly identifiable in the absence of the *PXf*, *ER* and *ERL2*, and they remained present, albeit lacking orientation and at a much reduced frequency in *pxf erf* lines (Fig. 6E-F). Thus, although not an absolute necessity for formation of either phloem or xylem vessels, these receptor-kinase families are absolutely essential in specifying their positioning and in coordinating cell division in a manner that allows organised radial expansion and pattern maintenance (Fig. 6).

Cell size in hypocotyls is balanced by *PXf* and *ERf*

One common characteristic of mutants with reduced cell division is an increase in cell size, relative to wild-type plants. This compensates for fewer cells, such that final organ size is often similar to that of wild-type plants (Horiguchi and Tsukaya, 2011). In the course of our hypocotyl analysis, cell sizes and shapes appeared to differ among our mutant lines, and, in particular, cells in *pxf* lines appeared larger than those of other lines (Fig. 3A,B). Consequently, cell morphology was calculated from images of anatomical sections by selecting cell representatives from the different genotypes and using a MATLAB code to analyse the cells as connected components with measurable features (Fig. S6A,B). Cell area and perimeter were investigated for xylem vessels, fibres, xylem parenchyma and phloem cells in wild-type, *pxf*, *pxf er erl1*, *pxf er erl2*, and *pxf erf* lines (Fig. 7) with one exception. Fibre morphology could not be assessed in *pxf erf*, as insufficient fibre cells were present (Fig. 6F). In hypocotyls, all *pxf* cell types tested demonstrated increases in cell perimeter relative to wild type (Fig. 7; Table S4). *pxf er* and *pxf* cells demonstrated no statistically significant differences in vessel, fibre and phloem cell perimeters, but *pxf er* xylem parenchyma perimeters were smaller than those of *pxf* lines. Strikingly, removal of further members of the ERf restored vessel, parenchyma and phloem cell perimeters to wild-type sizes (Fig. 7A,B,D; Table S4). Thus members of the *ERf* are required to promote increases in cell size in the absence of *PXf*.

The one cell type that was the exception to this cell size regulation was xylem fibres. Here, the increase in fibre perimeter that was characteristic of *pxf* mutant hypocotyl cells was not rescued by *erf* mutants (Fig. 7C; Table S4). These observations were supported by cell area measurements. For the four cell types tested, *pxf* cell areas were larger than those of wild-type plants but, with the exception of fibres, removal of *er erl1* or *er erl2* from *pxf* restored cell areas to those observed in wild type (Fig. 7; Table S5).

Xylem cells are characterised by rigid secondary cell walls, so we hypothesised that parenchyma may be subject to changes in cell shape to accommodate the increased xylem cell size. To test this hypothesis, we calculated the ellipticity of the parenchyma and other hypocotyl cell types by determining their major to minor axis ratios in wild-type, *pxF* and *pxF er erl2* lines. However, this parameter varied little between genotypes (Fig. S6C-F).

Phenotypes of *pxf erf* sextuple mutant stems

To complete our analysis of *pxf erf* sextuple mutant morphology, we examined vascular tissue in inflorescence stems. Inflorescence stem vascular morphology was similar in *pxf erf* lines and *pxf er erl2* counterparts (Fig. 8). Both were characterised by very large reductions in vascular bundle size. Characteristic xylem and phloem cell types were present, but only very small xylem vessels were observed, relative to those found in wild-type, *erf* and *pxf* lines (Figs 8D,E and 9A; Tables S6 and S7). Furthermore, tissue layer

Development (2019) 146, dev177105. doi:10.1242/dev.177105

organisation defects were apparent beyond those previously observed. In particular, the clearly defined organisation of endodermal and adjacent phloem cap cells were lacking, with the phloem cap appearing to extend into the cortex (Fig. 8D) or be absent altogether (Fig. 8E). Thus, tissue layer defects occurred outwith vascular cell types. These similarities in vascular morphology were independent of plant size because gross morphology of *pxf erf* sextuple lines was considerably smaller than *pxf er erl2* counterparts (Fig. S7).

Having observed large reductions in xylem vessel size in stems (Fig. 9A), we tested whether *PXF* and *ERF* genes genetically interacted to control cellular morphology of other vascular cell types in the stem (Fig. 9B,C). In stems, xylem vessels and cells in the phloem were smaller in *pxf* lines than in wild type, as determined by measuring both cell perimeter and cell area, and in contrast to measurements in the hypocotyl. Removing *ER* from *pxf* lines resulted in no change to the size of these cells, but loss of *ERL2* from *pxf er* plants caused a further reduction in cell size (Fig. 9A,C; Tables S6 and S7). Thus, in phloem and xylem vessels, *pxf* and *erf* families interact to maintain cell size. Xylem fibre sizes differed from this trend. Here, *pxf er* cells were significantly larger than wild type, but this phenotype was suppressed in *pxf er erl2* plants as fibre perimeter and area was unchanged from wild type (Fig. 9B; Tables S6 and S7). We were unable to assess fibre morphology in *pxf erf* vascular bundles, as too few were identifiable in these lines (Fig. 8E). Taken together, our results demonstrate that a genetic interaction between PXF and ERF signalling coordinates organ size at the level of cell size, in addition to coordination of proliferation and pattern maintenance in both stems and hypocotyls.

DISCUSSION

Coordination of growth between cell layers

Plant growth and development require coordination between expanding tissue layers, particularly where tissue types are organised in concentric rings. Clearly, expansion of inner layers must be coordinated with expansion of outer layers. How does coordination between tissue layers occur? It was proposed some time ago that the *ERF* could perform this function (Shpak et al., 2004), and this initial suggestion has subsequently been supported by observations that, in the inflorescence stem, endodermis derived EPFL ligands signal to ER in the phloem to regulate cell division in the adjacent procambium (Uchida et al., 2012; Uchida and Tasaka, 2013) (Fig. 10A). Our observation that *PXL* expression is higher in the stem of *er* mutants (Fig. 1D) suggests that these endodermis-derived signals could act through ER to attenuate *PXF*-regulated vascular expansion (Fig. 10A). The alternative conclusion would be that *PXL* expression is higher in *er* mutants due to a change in stem morphology, but we regard this as unlikely for two reasons. First, there are negligible differences in vascular proliferation and organisation in *er* stem vascular tissue compared with wild type that could account for such changes in gene expression (Figs. 1E,F and 2A,B). Second, there is clear evidence that *pxl1* and *pxl2* genetically interact with *er*. This interaction is apparent in a *pxy* mutant background, as *pxf er* lines demonstrated fewer cells in stem vascular bundles than either *pxy er* or *pxf* lines (Fig. 2; Table S2).

Our experimentation with *pxf er* lines led to observations that *PXF* receptors, redundantly with *ER*, are required for normal expression levels of ERL receptors and their *EPFL* ligands in the stem (Fig. 3). As *CLL2* and *CHAL* are endodermis expressed, changes in the expression levels of these genes could be due to coordination of vascular tissue expansion in stems across multiple tissue layers via a series of feedback loops (Fig. 10). As the endodermal stem layer remains clearly defined in *er pxf* lines, it is unlikely that the reduction in *CHAL*/ and *CLL2* expression in these lines is due to the disruption of endodermal cell fate (Fig. 2F). However, owing to severe disruptions to vascular morphology adjacent to the endodermis, we cannot rule out that such changes are a consequence of the disruption to xylem, phloem and procambium organisation. Disruption to *pxf er* quadruple mutants was severe to such a degree that in stems, vascular tissue was no longer found in discrete bundles, but scattered around the stem adjacent to the endodermis (Fig. 2).

Oriented cell divisions and the development of organ boundaries in the rib zone of the shoot apical meristem, from which stem vascular tissue is derived, have been reported to be regulated by a homeodomain transcription factor, REPLUMLESS (RPL). Pertinent to the results obtained here, RPL was found to occupy the promoters of *PXY*, *CLE41*, *CLE42*, *ER*, *ERL1*, *ERL2* and *CHAL* in ChIP-Seq experiments (Bencivenga et al., 2016). RPL is localised to the cytoplasm unless present in a heterodimer with class I KNOX protein, such as BREVIPEDICELLUS (Bhatt et al., 2004). *rpl bp* double mutants, particularly those in the L*er* background that lacks a functional copy of *ER*, demonstrate considerable defects in vascular development (Etchells et al., 2012; Smith and Hake, 2003). Thus, events in the rib zone that are controlled by RPL could set up the initial pattern in the stem. Our genetic analysis demonstrates that however the pattern is initiated, it is maintained by interacting

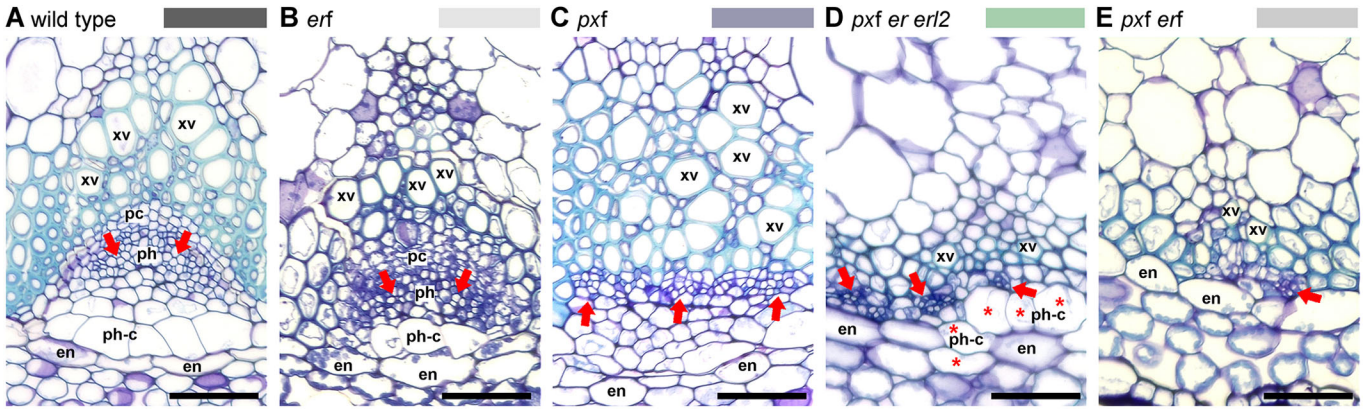

Fig. 8. Stem tissue from *pxf erf* lines. (A) Wild-type, (B) *erf*, (C) *pxf*, (D) *pxf er erl2*, (E) *pxf erf* vascular bundles. Phloem arrangement is marked with red arrows. Cells with phloem cap-like morphology are marked with asterisks. Scale bars: 50 µm; xv, xylem vessel; pc, procambium; ph, phloem; ph-c, phloem cap; en, endodermis.

Development (2019) 146, dev177105. doi:10.1242/dev.177105

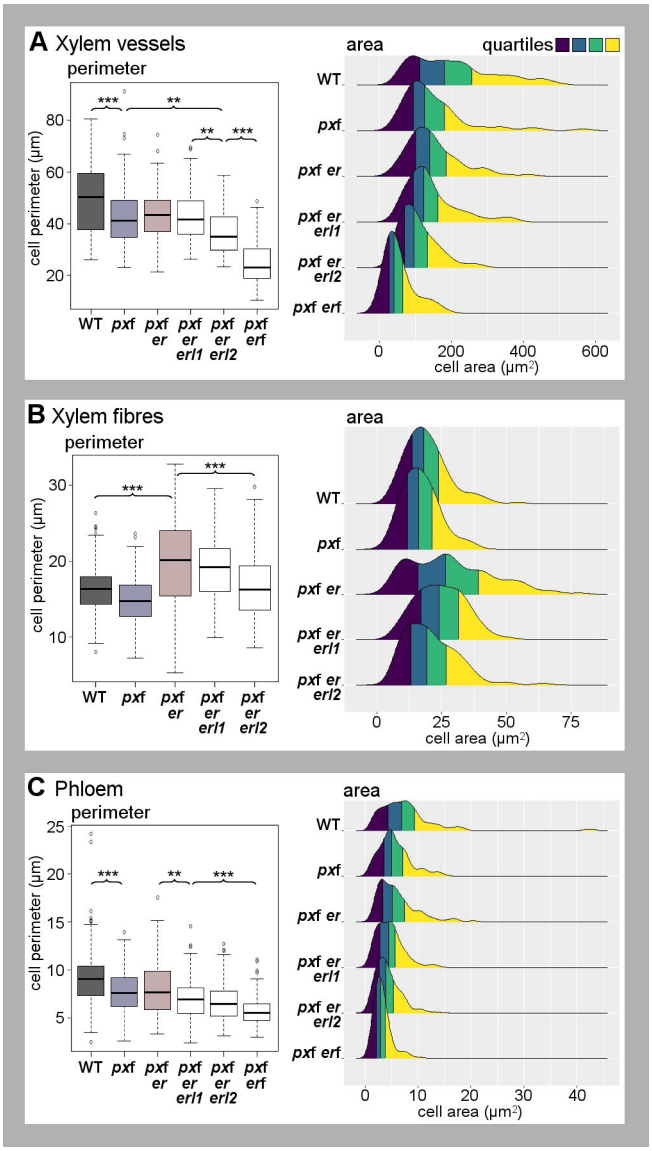

Fig. 9. Comparisons of morphology of cells in stem vascular bundles. (A-C) Boxplots on left show mean cell perimeter for xylem vessels (A), xylem fibres (B) and phloem cells (C). Boxes represent the 25th to 75th percentile, the horizontal line marks the median. Whiskers' endpoints are the min/max points within the interval spanning Q1-1.5*IQR (lower) and Q3-1.5*IQR (upper). Asterisks mark significant differences (ANOVA plus Tukey; ***P<0.001, **P<0.01; see Table S6 for pairwise comparisons of P values). Ridgeline plots on the right show the distributions of cell areas divided into quartiles. Areas of *pxf er* lines were greater than those of *pxf er erl2* lines in all three cell types ($P \leq 0.05$). Differences were calculated with ANOVA and a Tukey post-hoc test; see Table S7 for pairwise comparisons of P values.

signalling pathways characterised by members of the ERECTA and PXY families.

ERL genes are prominent in regulating cell size

Evidence that mechanisms exist to adjust cell morphology in order to maintain tissue size and organisation include the observation that cell expansion differs according to the rate of cell division. Here, overall organ size in mutants with fewer cells is often comparable to or only subtly different from those of wild-type plants due to an increase in cell size (De Veylder et al., 2002; Hemerly et al., 1999; Shpak et al., 2004; Ullah et al., 2001). Furthermore, such mechanisms can act non-

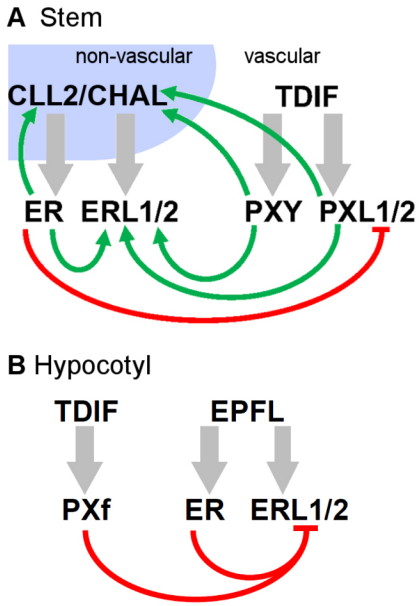

Fig. 10. Hypothesis of gene expression regulation in stems and hypocotyls. (A) In the stem, *ER* represses *PXL* gene expression. *PXf* and *ER* act as activators of ERL and *EPFL* gene expression. (B) In hypocotyls, negative regulation of *PXf* and *ER* targets predominate. Green arrows indicate a positive influence on gene expression; red blunt-ended lines indicate repression. Grey arrows indicate ligand-receptor interactions.

cell autonomously. Expression of *KRP1* reduces cell division (Hemerly et al., 1995). When it is specifically expressed in the epidermal cell layer, concomitant changes to palisade cell size and density also occur (Lehmeier et al., 2017). Thus, where the cell cycle has been manipulated in one cell layer, influence on cell size and organisation occurs in adjacent tissues, contributing to tissue integrity. We found that the interaction between *PXf* and *ERf* was crucial to regulation of cell size in multiple cell types. The ability to adjust cell size to compensate for the profound reductions in cell division in *pxf er* lines was particularly dependent on *ERL2* (Figs 7 and 9). This is in contrast to the consequences of losing the *ERECTA* family alone, as cell size adjustments are a feature of *erf* mutants (Shpak et al., 2004). However, the influence of *ERL2*, *ER* and *ERL1* differed by cell type and organ. In hypocotyls, vascular cells were larger in either *pxf* or *pxf er* lines compared with wild type. In hypocotyl xylem vessels, parenchyma and phloem cells, this increase in size was dependent on ERL gene expression as increases in cell size were lost in *pxf er erl1* and *pxf er erl2* lines (Fig. 7A,B,D). In stem vascular bundles, the only cell type with an increase in size in response to fewer to cell divisions were the fibres. This phenotype was also suppressed by removal of ERL genes. These observations support the idea that one function of the genetic interaction between *ERf* and *PXf* is coordination of tissue expansion. We propose that with these signalling mechanisms removed, the positional information that must be interpreted for cell morphology adjustments to occur is missing.

Genetic interactions may underpin physical interactions

In stems, the receptor kinases that are the focus of this study are expressed in discrete domains. By contrast, in hypocotyls, expression patterns of ER and PXY overlap on the xylem side of the cambium (Hirakawa et al., 2008; Ikematsu et al., 2017; Shi et al., 2019; Smetana et al., 2019). As the domain of ERL gene expression is expanded in *pxy* mutants (Fig. 5B,E,H), the presence

Development (2019) 146, dev177105. doi:10.1242/dev.177105

of PXL receptors in cells that also express ERf proteins is increasingly likely. A direct interaction between members of these receptor families is therefore possible. A recent *in vitro* global analysis of receptor kinase interactions did not include direct interactions between ERf and PXf family members because putative interactions did not pass cut-offs for inclusion in the high confidence bidirectional dataset (Smakowska-Luzan et al., 2018). Nevertheless strong *in vitro* interactions between ER and PXY, and ER and PXL1 proteins were observed in one orientation, and between PXL2 and ERL2 in both directions [Youssef Belkhadir, personal communication; data available in BAR ePlant (Waese et al., 2017)]. The determination of whether these interactions are genuine and, if so, the circumstances under which they occur *in vivo* will be an important focus for future research. ERf activity in the epidermis has previously been reported to be buffered by a second receptor, TOO MANY MOUTHS (TMM). Loss of this buffering in *tmm* mutants leads to opposite stomatal spacing phenotypes in spatially separate cotyledon, where stomata cluster, compared with hypocotyls where stomata are absent. Differing ligand availability in cotyledon and hypocotyl is thought to account for this difference (Abrash et al., 2011). CHAL and CLL2 have been demonstrated to act as ERf ligands in the inner tissues of stems (Uchida et al., 2012). We have shown that these ligands are expressed in developing xylem in hypocotyls (Fig. 1B,C). Thus, in stem vascular tissue, active ligand-ER complexes most likely reside in the phloem, whereas in hypocotyls they would be predominant in xylem initials. It remains to be determined whether the difference in ERL gene regulation by *ER* and *PXf* in stem and hypocotyl could be due to differing complements of co-receptors and ligands in these differing locations.

Our observation that ERL gene expression is de-repressed in the absence of *PXf* and *ER* in hypocotyls (Fig. 5J-K) supports the idea that these components genetically interact. Perhaps the most striking of our findings was the observation that *ER* and *PXf* regulation of ERL gene expression in the hypocotyl occurred in a manner opposite to that observed in the stem (compare Figs 4A,B and 5J,K), where *ER* and *PXf* combine to repress ERL gene expression. Thus, while *PXf* and *ERf* are required non-cell autonomously for tissue organisation and expansion in both stems and hypocotyls, the regulatory networks through which development is controlled in these two organs differs (Fig. 10). One explanation for differences in regulation is that tissue layer organisation varies by location. In hypocotyls, cambium division must occur concomitantly with factors that control periderm division. By contrast, in stems there is no such continually expanding tissue outside the vascular tissue, so vascular proliferation in stems must be under much tighter regulation.

PXf and *ERf* are an absolute requirement for hypocotyl secondary growth

Factors controlling the transition to secondary growth in *Arabidopsis* hypocotyls have recently been described. It first arises in cells adjacent to xylem, and central to this transition was an accumulation of auxin and expression of *HD-ZipIII* transcription factors. These factors, in turn, activate expression of *PXY* signalling (Smetana et al., 2019). Nevertheless, *pxy* mutants, and indeed *pxf* triple mutants, do ultimately make the transition to secondary growth (Figs 3 and 6). Thus, other factors must act with PXY to regulate the transition secondary growth and radial pattern in hypocotyls. *pxy er* double mutants, *erf* triple mutants, *pxf er* quads, and both *pxf er erl1* and *pxf er erl2* quintuple lines all made the transition to full secondary growth (Figs 4 and 6). By contrast, *pxf erf* sextuple mutants did not. As such, these lines demonstrated a phenotype that, as far as we are aware, has never previously been described. The observation of this novel phenotype further supports the idea that these receptor families coordinate development through a genetic interaction, and that the phenotypes cannot be explained simply by a correlative loss of cell division-promoting factors. Thus, PXf and ERf signalling act redundantly to regulate radial growth transition; consequently, complete removal of *PXf* and *ERf* families results not only in prominent proliferation defects, but also in dramatic defects to patterning (Fig. 6).

Concluding remarks

In *Arabidopsis*, stem and hypocotyl differ in that the hypocotyl undergoes radial growth, but the vast majority of the stem does not. Radial hypocotyl growth is largely the consequence of expansion of a pattern that is laid down in the embryo, but in stems, *de novo* patterning must occur below the shoot apical meristem. Nevertheless, in both stem and hypocotyl, the xylem, (pro)cambium and phloem must be specified in adjacent tissue layers in a coordinated manner. Our mutant analysis demonstrates that interactions between *PXf* and *ERf* are central to maintaining this organisation by regulating cell division (Figs 6 and 8) and coordinating cell size (Figs 7 and 9) in these different contexts.

MATERIALS AND METHODS

Accession numbers

AGI accession numbers for the genes studies in this manuscript are as follows: At3g24770 (*CLE41*), At5g61480 (*PXY*), At1g08590 (*PXL1*), At4g28650 (*PXL2*), At2g26330 (*ER*), At5g62230 (*ERL1*), At5g07180 (*ERL2*), At4g14723 (*CLL2*/*EPFL4*), At3g22820 (*CLL1*/*EPFL5*) and At2g30370 (*CHAL*/*EPFL6*).

Gene expression

For qRT-PCR, RNA was isolated using Trizol reagent (Life Technologies) prior to DNAse treatment with RQ1 (Promega). cDNA synthesis was performed using Tetro reverse transcriptase (Bioline). All samples were measured in technical triplicates on biological triplicates. qPCR reactions were performed using qPCRBIO SyGreen Mix (PCR Biosystems) using a CFX connect real-time system (Bio-Rad) with the standard sybr green detection programme. A melting curve was produced at the end of every experiment to ensure that only single products were formed. Gene expression was determined using a version of the comparative threshold cycle (Ct) method using average amplification efficiencies of each target, as determined using LinReg PCR software (Ramakers et al., 2003). Samples were normalised to *18S* rRNA or *ACT2*. Primers for qRT-PCR are described in Table S1. Significant differences in gene expression were identified with ANOVA and an LSD post-hoc test for four-way comparisons or using Student's *t*-test for two-way comparisons.

Plant lines

Previously described parental lines *pxy-3 pxl1-1 pxl2-1* (referred to hereafter as *pxf*) and *pxy-5 er-124* (Etchells et al., 2013) were crossed to generate *pxy-3 pxl1-1 pxl2-1 er-124* (*er pxf*). The quadruple mutants were selected in F3 by PCR using primers listed in Table S8. To generate *pxf er erl2* quintuple mutants, parental lines *er-105 erl1-2/+ erl2-1* (*erf*) (Shpak et al., 2004) and *pxy-3 pxl1-1 pxl2-1* (Etchells et al., 2013) were crossed. Plants homozygous for *er* were selected by visual phenotype in the F2, which was also sprayed with glufosinate to select for plants carrying an *erl2-1* allele. Families homozygous for glufosinate resistance in the F3 were screened for *pxy-3*, *pxl1-1* and *pxl2-1* to generate *pxf er erl2*. *er* and *erl2* mutants were subsequently confirmed by PCR.

erl1 genome edited lines were generated using an egg cell-specific CRISPR/Cas9 construct (Wang et al., 2015; Xing et al., 2014). Briefly, target sequences TCCAATTGCAGAGACTTGCAAGG and TCTTGCT-GGCAATCATCTAACGG were identified using the CRISPR-PLANT

website (Xie et al., 2014) and tested for off-targets (Bae et al., 2014). Primers incorporating the target sequences (Table S8) were used in a PCR reaction with plasmid pCBC-DT1T2 as a template to generate a PCR product incorporating a guide RNA against *ERL1*. A golden gate reaction was used to incorporate the purified PCR product into pHEE2E-TRI. The resultant *ERL1* CRISPR/cas9 clone was transferred to *Arabidopsis* by floral dip (Clough and Bent, 1998). *erl1*^{GE} mutants were selected in the T1 generation by sequencing PCR products generated from primers specific to ERL1 genomic DNA that flanked the guide RNA target sites.

For spatial expression of *ER*f genes in *pxy* or *er*, previously described *ER::GUS*, *ERL1::GUS* and *ERL2::GUS* reporters were used (Shpak et al., 2004). These were crossed to *pxy-3* or *er-124*. *pxy* mutants were selected in the F2 using primers described Table S8. Reporter lines were picked that also demonstrated GUS expression as judged by *GUS* histochemical staining, and the presence of *GUS* reporter construct was subsequently confirmed by PCR using primers (Table S8). For determination of ER-ligand expression, previously described *CHAL::GUS* and *CLL2::GUS* lines were used (Abrash et al., 2011).

Analysis of vascular tissue anatomy

Vascular morphology was assessed using tissue embedded in JB4 resin. For vascular bundles, inflorescence stem tissue from 0.5 cm above the rosette was assessed. Tissue was fixed in FAA, dehydrated in ethanol and infiltrated with JB4 infiltration medium, prior to embedding. Sections (4 µm) taken using a Thermo Fisher Scientific Finesse ME 240 microtome were stained in 0.02% aqueous Toluidine Blue and mounted with histomount.

GUS-stained tissue was harvested to ice-cold phosphate buffer. Samples were treated with ice-cold acetone for 5 min and then returned to phosphate buffer. GUS staining buffer (50 mM phosphate buffer, 0.2% triton, 2 mM potassium ferrocyanide, 2 mM potassium ferricyanide and 2 mM X-Gluc) was added and samples were infiltrated using a vacuum, before incubation overnight at 37ºC. Samples were progressively incubated in: FAA, then 70%, 85% and 95% ethanol for 30 min each prior to embedding in Technovit 7100 according to the manufacturer's instructions. Embedded samples were allowed to polymerize at room temperature for 2 h and at 37°C overnight. The inhibition layer was removed by wiping with a lint-free cloth. Samples were sectioned, counterstained with 0.1% Neutral Red and mounted using histomount.

Quantitative morphology calculations

To capture measurements for the cell perimeters and areas, images from six different individuals were selected for each genotype tested. A minimum of 10 cells of each cell type (xylem vessels, xylem fibres, phloem and parenchyma) were selected from a wedge with a 60° central angle from each image (Fig. S6A). Cells of each type were selected along the full length of the radial axis to ensure that cells of all sizes and phenotypic variation were represented. A MATLAB code (available on request) was generated to extract the intrinsic properties of each cell type. To that end, the code was designed to split each image into binary sub-images, wherein the interior of the cell type of interest was represented as white objects on black background (Fig. S6B). The cells (the white objects) from each image were then analysed as connected components of the image and their area and perimeter extracted. To remove noise, i.e. data obtained from objects that were wrongly classified as connected components within the algorithm (e.g. stray pixels), the code was devised to discard data that yielded unrealistically small values for perimeter and area (perimeter value of 0 µm, area smaller than 1 µm^2). The data were converted from pixels to µm using a calibration factor, in order to yield results consistent with laboratory observations. For each cell type, an equal number of cells was selected on a random basis from each plant within each genotype to avoid small variations between the number of representatives obtained from each individual plant.

To test the significance of the variation between the cell areas and perimeters between the different genotypes, a nested ANOVA was performed in R at 5% significance level. To perform the nested ANOVA, the data were classified according to genotype (treatment) and plant ID (plants within that treatment), with the response variable either the area or perimeter. A post-hoc Tukey HSD test was performed to determine the significance of the pairwise differences between the means of the areas/perimeters between the different genotypes. To determine the reliability of the results, the residuals from the data were tested for normality. Histograms and quantile-quantile plots for the residuals of each cell type were used to judge the distribution, followed by a Shapiro-Wilk normality test. The residuals for the data for all cell types withstood the Shapiro-Wilk normality test at 5% significance level, confirming that the results of the ANOVA analysis were reliable.

Mean hypocotyl diameters were measured using callipers. The radius was calculated from hypocotyl images of six plants from each genotype. A MATLAB code was used to measure the length of the shorter radius. The length of the radii in pixels was subsequently converted to µm. A Lilliefors test at 5% significance level was used to confirm that the radii for each genotype were normally distributed. A one-way ANOVA followed by a post-hoc Tukey HSD test was used to determine pairwise variation between the means.

Acknowledgements

We thank Miguel de Lucas, Keith Lindsey and Jen Topping for critical reading of the manuscript, and Youssef Belkhadir for comments on the preprint. The authors are grateful to Keiko Torii for sharing *er* and *erl* mutants, and *ER*f reporter lines, and to the Nottingham Arabidopsis Stock Centre for providing other genetic resources.

Competing interests

The authors declare no competing or financial interests.

Author contributions

Conceptualization: J.P.E.; Software: K.S.B., I.H.J.; Formal analysis: J.P.E.; Investigation: N.W., K.S.B., R.E.D., X.Y.W., J.T.K., K.A.C., J.P.E.; Writing - original draft: J.P.E.; Writing - review & editing: K.S.B., R.E.D., I.H.J., S.R.T.; Supervision: W.W., I.H.J., S.R.T., J.P.E.; Project administration: J.P.E.; Funding acquisition: S.R.T., J.P.E.

Funding

This work was funded by the European Union (329978, a Marie Skladowska Curie Fellowship to J.P.E.), by the Biotechnology and Biological Sciences Research Council (BB/H019928 to J.P.E. and S.R.T., and a NLD-DTP studentship to K.S.B., J.P.E. and I.H.J.), and by an N8 AgriFood programme grant to J.P.E. and S.R.T. The authors gratefully acknowledge a travel grant from Henan Agricultural University to N.W.

Supplementary information

Supplementary information available online at
http://dev.biologists.org/lookup/doi/10.1242/dev.177105.supplemental

References

Abrash, E. B., Davies, K. A. and Bergmann, D. C. (2011). Generation of signaling specificity in arabidopsis by spatially restricted buffering of ligand–receptor interactions. *Plant Cell* **23**, 2864-2879. doi:10.1105/tpc.111.086637

Bae, S., Park, J. and Kim, J.-S. (2014). Cas-OFFinder: a fast and versatile algorithm that searches for potential off-target sites of Cas9 RNA-guided endonucleases. *Bioinformatics* **30**, 1473-1475. doi:10.1093/bioinformatics/btu048

Bemis, S. M., Lee, J. S., Shpak, E. D. and Torii, K. U. (2013). Regulation of floral patterning and organ identity by Arabidopsis ERECTA-family receptor kinase genes. *J. Exp. Bot.* **64**, 5323-5333. doi:10.1093/jxb/ert270

Bencivenga, S., Serrano-Mislata, A., Bush, M., Fox, S. and Sablowski, R. (2016). Control of oriented tissue growth through repression of organ boundary genes promotes stem morphogenesis. *Dev. Cell* **39**, 198-208. doi:10.1016/j.devcel.2016.08.013

Bhatt, A. M., Etchells, J. P., Canales, C., Lagodienko, A. and Dickinson, H. (2004). VAAMANA–a BEL1-like homeodomain protein, interacts with KNOX proteins BP and STM and regulates inflorescence stem growth in Arabidopsis. *Gene* **328**, 103-111. doi:10.1016/j.gene.2003.12.033

Chaffey, N., Cholewa, E., Regan, S. and Sundberg, B. (2002). Secondary xylem development in Arabidopsis: a model for wood formation. *Physiol. Plant* **114**, 594-600. doi:10.1034/j.1399-3054.2002.1140413.x

Clough, S. J. and Bent, A. F. (1998). Floral dip: a simplified method for Agrobacterium-mediated transformation of Arabidopsis thaliana. *Plant J.* **16**, 735-743. doi:10.1046/j.1365-313x.1998.00343.x

De Veylder, L., Beeckman, T., Beemster, G. T. S., Engler, J. D., Ormenese, S., Maes, S., Naudts, M., Van der Schueren, E., Jacqmard, A., Engler, G. et al. (2002). Control of proliferation, endoreduplication and differentiation by the Arabidopsis E2Fa-DPa transcription factor. *EMBO J.* **21**, 1360-1368. doi:10.1093/emboj/21.6.1360

Dolan, L., Janmaat, K., Willemsen, V., Linstead, P., Poethig, S., Roberts, K. and Scheres, B. (1993). Cellular-organization of the arabidopsis-thaliana root. *Development* **119**, 71-84.

Efroni, I., Mello, A., Nawy, T., Ip, P.-L., Rahni, R., DelRose, N., Powers, A., Satija, R. and Birnbaum, K. D. (2016). Root regeneration triggers an embryo-like sequence guided by hormonal interactions. *Cell* **165**, 1721-1733. doi:10.1016/j.cell.2016.04.046

Etchells, J. P. and Turner, S. R. (2010). The PXY-CLE41 receptor ligand pair defines a multifunctional pathway that controls the rate and orientation of vascular cell division. *Development* **137**, 767-774. doi:10.1242/dev.044941

Etchells, J. P., Moore, L., Jiang, W. Z., Prescott, H., Capper, R., Saunders, N. J., Bhatt, A. M. and Dickinson, H. G. (2012). A role for BELLRINGER in cell wall development is supported by loss-of-function phenotypes. *BMC Plant Biol.* **12**, 212. doi:10.1186/1471-2229-12-212

Etchells, J. P., Provost, C. M., Mishra, L. and Turner, S. R. (2013). WOX4 and WOX14 act downstream of the PXY receptor kinase to regulate plant vascular proliferation independently of any role in vascular organisation. *Development* **140**, 2224-2234. doi:10.1242/dev.091314

Fisher, K. and Turner, S. (2007). PXY, a receptor-like kinase essential for maintaining polarity during plant vascular-tissue development. *Curr. Biol.* **17**, 1061-1066. doi:10.1016/j.cub.2007.05.049

Han, S., Cho, H., Noh, J., Qi, J., Jung, H.-J., Nam, H., Lee, S., Hwang, D., Greb, T. and Hwang, I. (2018). BIL1-mediated MP phosphorylation integrates PXY and cytokinin signalling in secondary growth. *Nat. Plants* **4**, 605-614. doi:10.1038/s41477-018-0180-3

Hemerly, A., Engler, J. D. A., Bergounioux, C., Van Montagu, M., Engler, G., Inzé, D. and Ferreira, P. (1995). Dominant negative mutants of the Cdc2 kinase uncouple cell division from iterative plant development. *EMBO J.* **14**, 3925-3936. doi:10.1002/j.1460-2075.1995.tb00064.x

Hemerly, A. S., Ferreira, P. C. G., Van Montagu, M. and Inze, D. (1999). Cell cycle control and plant morphogenesis: is there an essential link? *BioEssays* **21**, 29-37 doi:10.1002/(SICI)1521-1878(199901)21:1

Hirakawa, Y., Shinohara, H., Kondo, Y., Inoue, A., Nakanomyo, I., Ogawa, M., Sawa, S., Ohashi-Ito, K., Matsubayashi, Y. and Fukuda, H. (2008). Non-cell-autonomous control of vascular stem cell fate by a CLE peptide/receptor system. *Proc. Natl. Acad. Sci. USA* https://www.ncbi.nlm.nih.gov/pubmed/?term=Non-cell-autonomous+control+of+vascular+stem+cell+fate+by+a+CLE+peptide%2Freceptor+system **105**, 15208-15213. doi:10.1073/pnas.0808444105

Hirakawa, Y., Kondo, Y. and Fukuda, H. (2010). TDIF peptide signaling regulates vascular stem cell proliferation via the WOX4 homeobox gene in arabidopsis. *Plant Cell* **22**, 2618-2629. doi:10.1105/tpc.110.076083

Horiguchi, G. and Tsukaya, H. (2011). Organ size regulation in plants: insights from compensation. *Front. Plant Sci.* https://www.ncbi.nlm.nih.gov/pubmed/?term=Organ+size+regulation+in+plants%3A+insights+from+compensation **2**, 24. doi:10.3389/fpls.2011.00024

Ikematsu, S., Tasaka, M., Torii, K. U. and Uchida, N. (2017). ERECTA-family receptor kinase genes redundantly prevent premature progression of secondary growth in the Arabidopsis hypocotyl. *New Phytol.* **213**, 1697-1709. doi:10.1111/nph.14335

Ito, Y., Nakanomyo, I., Motose, H., Iwamoto, K., Sawa, S., Dohmae, N. and Fukuda, H. (2006). Dodeca-CLE peptides as suppressors of plant stem cell differentiation. *Science* **313**, 842-845. doi:10.1126/science.1128436

Kajala, K., Ramakrishna, P., Fisher, A., Bergmann, D. C., De Smet, I., Sozzani, R., Weijers, D. and Brady, S. M. (2014). Omics and modelling approaches for understanding regulation of asymmetric cell divisions in arabidopsis and other angiosperm plants. *Ann. Bot.* **113**, 1083-1105. doi:10.1093/aob/mcu065

Kimura, Y., Tasaka, M., Torii, K. U. and Uchida, N. (2018). ERECTA-family genes coordinate stem cell functions between the epidermal and internal layers of the shoot apical meristem. *Development* **145**, dev156380. doi:10.1242/dev.156380

Kondo, Y., Ito, T., Nakagami, H., Hirakawa, Y., Saito, M., Tamaki, T., Shirasu, K. and Fukuda, H. (2014). Plant GSK3 proteins regulate xylem cell differentiation downstream of TDIF–TDR signalling. *Nat. Commun.* **5**, 3504. doi:10.1038/ncomms4504

Lehmeier, C., Pajor, R., Lundgren Marjorie, R., Mathers, A., Sloan, J., Bauch, M., Mitchell, A., Bellasio, C., Green, A., Bouyer, D. et al. (2017). Cell density and airspace patterning in the leaf can be manipulated to increase leaf photosynthetic capacity. *Plant J.* **92**, 981-994. doi:10.1111/tpj.13727

Ragni, L., Nieminen, K., Pacheco-Villalobos, D., Sibout, R., Schwechheimer, C. and Hardtke, C. S. (2011). Mobile gibberellin directly stimulates arabidopsis hypocotyl xylem expansion. *Plant Cell* **23**, 1322-1336. doi:10.1105/tpc.111.084020

Ramakers, C., Ruijter, J. M., Deprez, R. H. L. and Moorman, A. F. M. (2003). Assumption-free analysis of quantitative real-time polymerase chain reaction (PCR) data. *Neurosci. Lett.* **339**, 62-66. doi:10.1016/S0304-3940(02)01423-4

Shi, D., Lebovka, I., López-Salmerón, V., Sanchez, P. and Greb, T. (2019). Bifacial cambium stem cells generate xylem and phloem during radial plant growth. *Development* **146**, dev171355. doi:10.1242/dev.171355

Shpak, E. D., Lakeman, M. B. and Torii, K. U. (2003). Dominant-negative receptor uncovers redundancy in the Arabidopsis ERECTA leucine-rich repeat receptor-like kinase signaling pathway that regulates organ shape. *Plant Cell* **15**, 1095-1110. doi:10.1105/tpc.010413

Shpak, E. D., Berthiaume, C. T., Hill, E. J. and Torii, K. U. (2004). Synergistic interaction of three ERECTA-family receptor-like kinases controls Arabidopsis organ growth and flower development by promoting cell proliferation. *Development* **131**, 1491-1501. doi:10.1242/dev.01028

Shpak, E. D., McAbee, J. M., Pillitteri, L. J. and Torii, K. U. (2005). Stomatal patterning and differentiation by synergistic interactions of receptor kinases. *Science* **309**, 290-293. doi:10.1126/science.1109710

Smakowska-Luzan, E., Mott, G. A., Parys, K., Stegmann, M., Howton, T. C., Layeghifard, M., Neuhold, J., Lehner, A., Kong, J., Grünwald, K. et al. (2018). An extracellular network of Arabidopsis leucine-rich repeat receptor kinases. *Nature* **553**, 342. doi:10.1038/nature25184

Smetana, O., Mäkilä, R., Lyu, M., Amiryousefi, A., Sánchez Rodríguez, F., Wu, M.-F., Solé-Gil, A., Leal Gavarrón, M., Siligato, R., Miyashima, S. et al. (2019). High levels of auxin signalling define the stem-cell organizer of the vascular cambium. *Nature* **565**, 485-489. doi:10.1038/s41586-018-0837-0

Smith, H. M. S. and Hake, S. (2003). The interaction of two homeobox genes, BREVIPEDICELLUS and PENNYWISE, regulates internode patterning in the arabidopsis inflorescence. *Plant Cell* **15**, 1717-1727. doi:10.1105/tpc.012856

Suer, S., Agusti, J., Sanchez, P., Schwarz, M. and Greb, T. (2011). WOX4 imparts auxin responsiveness to cambium cells in arabidopsis. *Plant Cell* **23**, 3247-3259. doi:10.1105/tpc.111.087874

ten Hove, C. A., Lu, K.-J. and Weijers, D. (2015). Building a plant: cell fate specification in the early Arabidopsis embryo. *Development* **142**, 420-430. doi:10.1242/dev.111500

Torii, K. U., Mitsukawa, N., Oosumi, T., Matsuura, Y., Yokoyama, R., Whittier, R. F. and Komeda, Y. (1996). The arabidopsis ERECTA gene encodes a putative receptor protein kinase with extracellular leucine-rich repeats. *Plant Cell* **8**, 735-746. doi:10.1105/tpc.8.4.735

Uchida, N. and Tasaka, M. (2013). Regulation of plant vascular stem cells by endodermis-derived EPFL-family peptide hormones and phloem-expressed ERECTA-family receptor kinases. *J. Exp. Bot.* **64**, 5335-5343. doi:10.1093/jxb/ert196

Uchida, N., Lee, J. S., Horst, R. J., Lai, H.-H., Kajita, R., Kakimoto, T., Tasaka, M. and Torii, K. U. (2012). Regulation of inflorescence architecture by intertissue layer ligand–receptor communication between endodermis and phloem. *Proc. Natl. Acad. Sci. USA* **109**, 6337-6342. doi:10.1073/pnas.1117537109

Uchida, N., Shimada, M. and Tasaka, M. (2013). ERECTA-Family Receptor Kinases Regulate Stem Cell Homeostasis via Buffering its Cytokinin Responsiveness in the Shoot Apical Meristem. *Plant Cell Physiol.* **54**, 343-351. doi:10.1093/pcp/pcs109

Ullah, H., Chen, J.-G., Young, J. C., Im, K.-H., Sussman, M. R. and Jones, A. M. (2001). Modulation of cell proliferation by heterotrimeric G protein in arabidopsis. *Science* **292**, 2066-2069. doi:10.1126/science.1059040

Waese, J., Fan, J., Pasha, A., Yu, H., Fucile, G., Shi, R., Cumming, M., Kelley, L. A., Sternberg, M. J., Krishnakumar, V. et al. (2017). ePlant: visualizing and exploring multiple levels of data for hypothesis generation in plant biology. *Plant Cell* **29**, 1806-1821. doi:10.1105/tpc.17.00073

Wang, Z.-P., Xing, H.-L., Dong, L., Zhang, H.-Y., Han, C.-Y., Wang, X.-C. and Chen, Q.-J. (2015). Egg cell-specific promoter-controlled CRISPR/Cas9 efficiently generates homozygous mutants for multiple target genes in Arabidopsis in a single generation. *Genome Biol.* **16**, 144. doi:10.1186/s13059-015-0715-0

Wunderling, A., Ripper, D., Barra-Jimenez, A., Mahn, S., Sajak, K., Targem, M. B. and Ragni, L. (2018). A molecular framework to study periderm formation in Arabidopsis. *New Phytol.* **219**, 216-229. doi:10.1111/nph.15128

Xie, K., Zhang, J. and Yang, Y. (2014). Genome-wide prediction of highly specific guide RNA spacers for CRISPR–Cas9-mediated genome editing in model plants and major crops. *Mol. Plant* **7**, 923-926. doi:10.1093/mp/ssu009

Xing, H.-L., Dong, L., Wang, Z.-P., Zhang, H.-Y., Han, C.-Y., Liu, B., Wang, X.-C. and Chen, Q.-J. (2014). A CRISPR/Cas9 toolkit for multiplex genome editing in plants. *BMC Plant Biol.* **14**, 327. doi:10.1186/s12870-014-0327-y

Zhang, H., Lin, X., Han, Z., Qu, L.-J. and Chai, J. (2016). Crystal structure of PXY-TDIF complex reveals a conserved recognition mechanism among CLE peptide-receptor pairs. *Cell Res.* **26**, 543. doi:10.1038/cr.2016.45

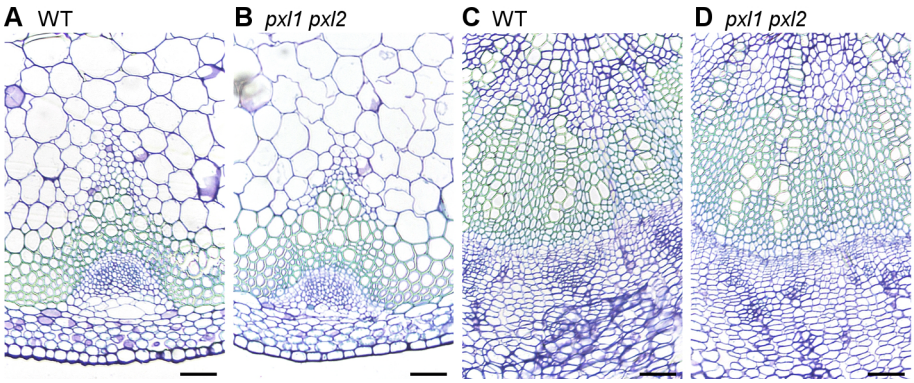

Figure S1. *pxl1 pxl2* vascular tissue is indistinguishable from wild type. Inflorescence stem vascular bundles from wild type plants (A) and *pxl1 pxl2* lines (B). Hypocotyl transverse sections from wild type (C) and *pxl1 pxl2* plants (D). Scales are 50 µM.

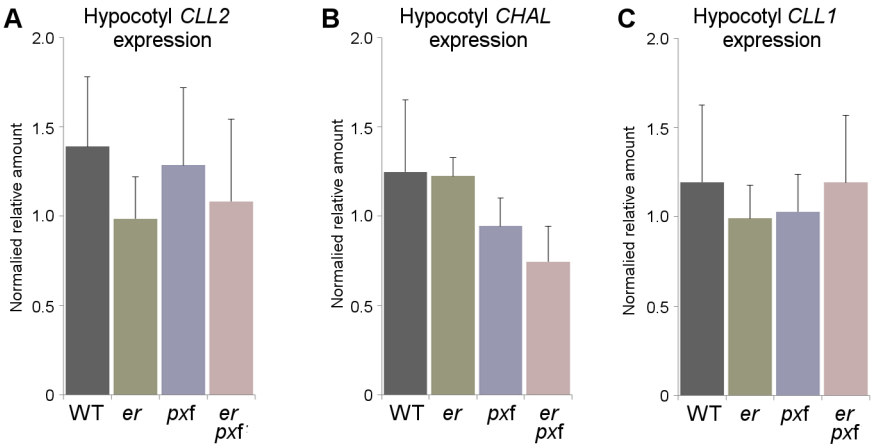

Figure S2. *EPFL* expression in hypocotyls. (A-C) Hypocotyl expression of *CLL2* (A), *CHAL* (B) and *CLL1* (C) in wild type, *er*, and *pxf* mutants (expression normalised to 18S rRNA). No significant differences in expression were observed, using ANOVA and LSD post-hoc test.

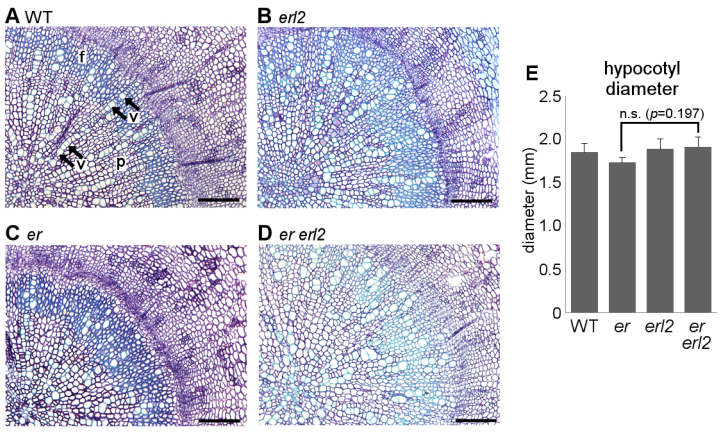

Figure S3. *er* and *erl2* mutant hypocotyl phenotypes. (A-D) Hypocotyl transverse sections of wild type (A), *erl2* (B), *er* (C), and *er erl2* (D) lines. (E) Graph showing hypocotyl diameter or *er erl2* lines and controls at 5 weeks old. Xylem fibres are marked 'f'; black arrows (v) mark vessels; 'p' marks parenchyma. Scales are 100 µM. *p* values were calculated with ANOVA and LSD post-hoc test.

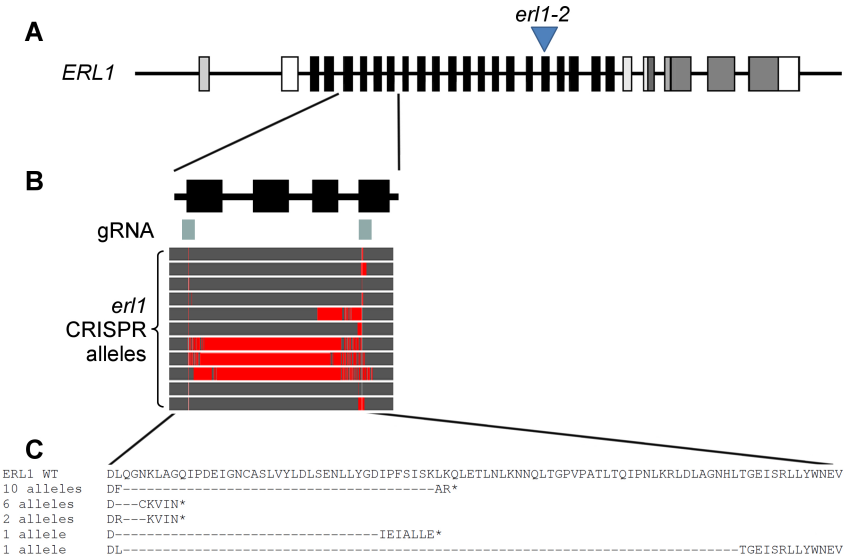

Figure S4. Diagram showing CRISPR/Cas9 generated *erl1* alleles. (A) Diagram showing intron-exon structure of *ERL1* with position of commonly used *erl1-2* allele marked with a blue triangle. (B) Close up of exons 5-8 showing positions of guide RNA (grey-green boxes), and the alleles identifies in the family analysed. Grey represents alignment with wild type sequence; red shows no alignment. (C) Translation of wild type and mutant *erl1* alleles. All but one has premature stop codons; the remaining allele has a large deletion of the LRR domain.

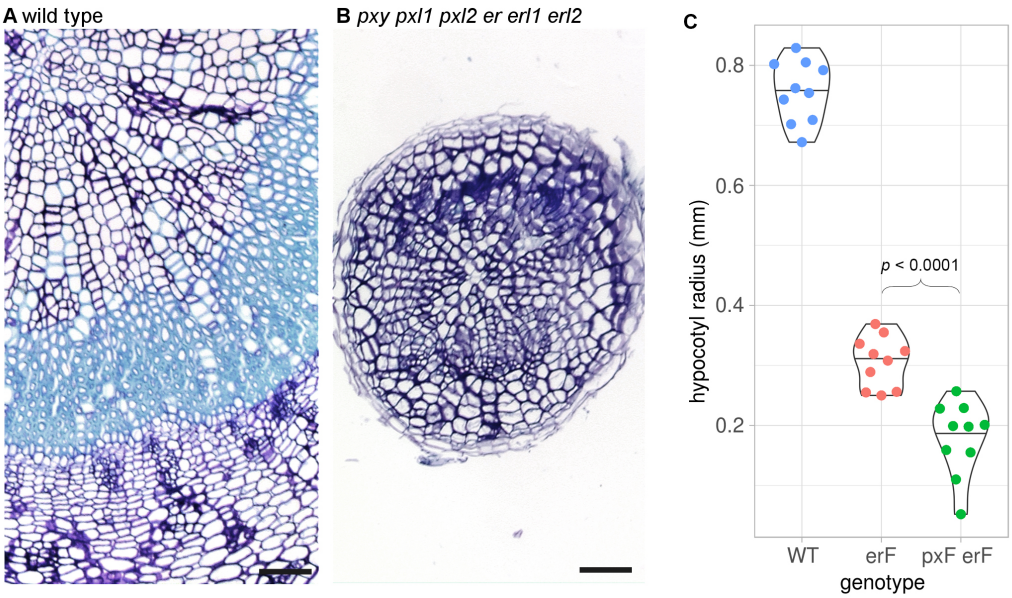

Figure S5. *pxf erf* hypocotyls. Close-up of wild type (A) and *pxf erf* (B) hypocotyls. Scales are 50 µM. (C) Violin plot showing comparison of *pxf* and *pxf erf* hypocotyl radii. *p* values were calculated with ANOVA and LSD post-hoc test.

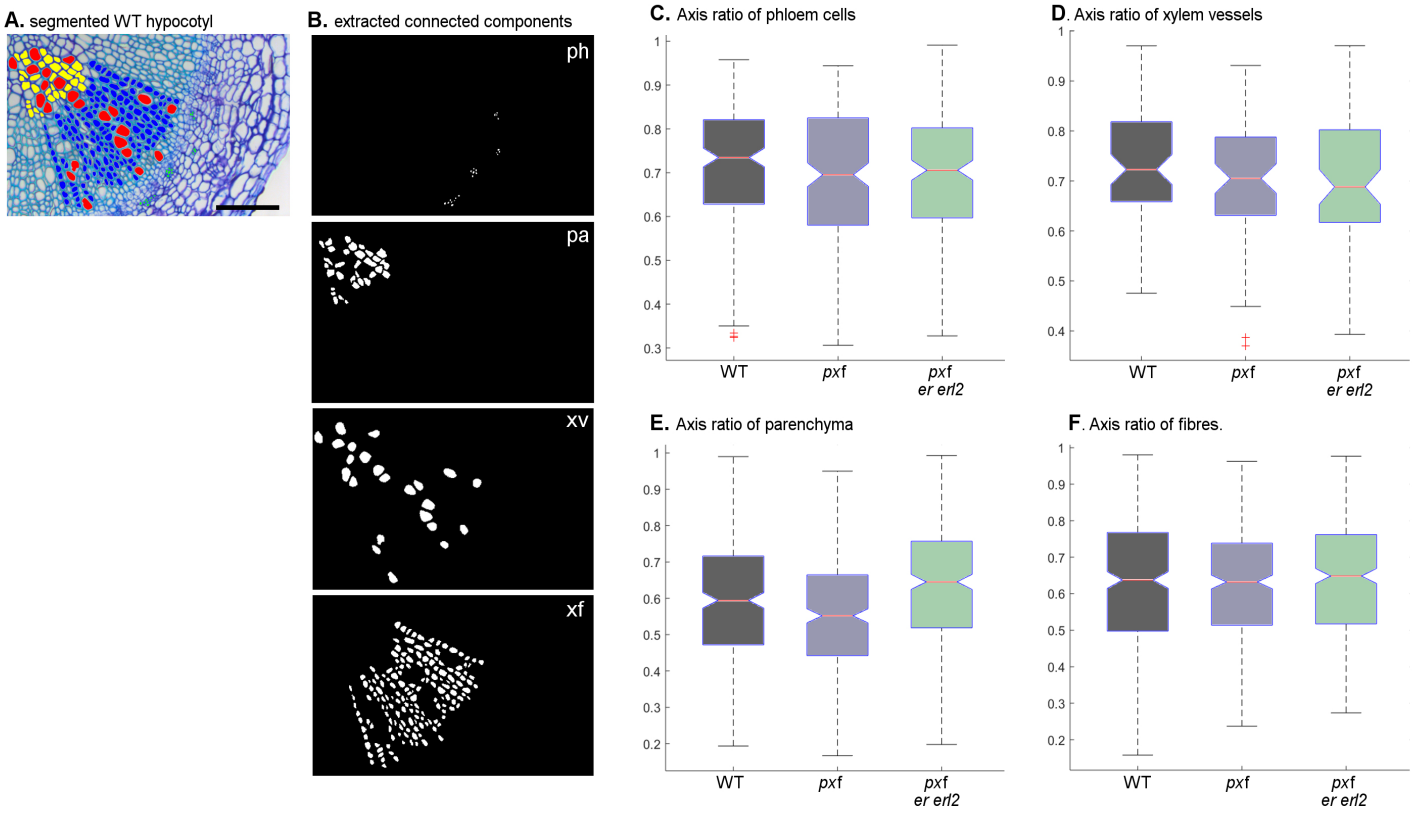

Figure S6. Example of extracted connected components. (A-B) Wild type hypocotyl with cell types segmented (xylem parenchyma are yellow; xylem fibres are blue; xylem vessels are red; phloem are green; A). Scale is 100 µM. (B) extracted connected components. (C-F) Notched box plot showing comparison of elipticity from extracted connected components for phloem (C), xylem vessels (D), parenchyma (E), and fibres (F) from wild type, *pxf*, and *pxf er erl2* lines.

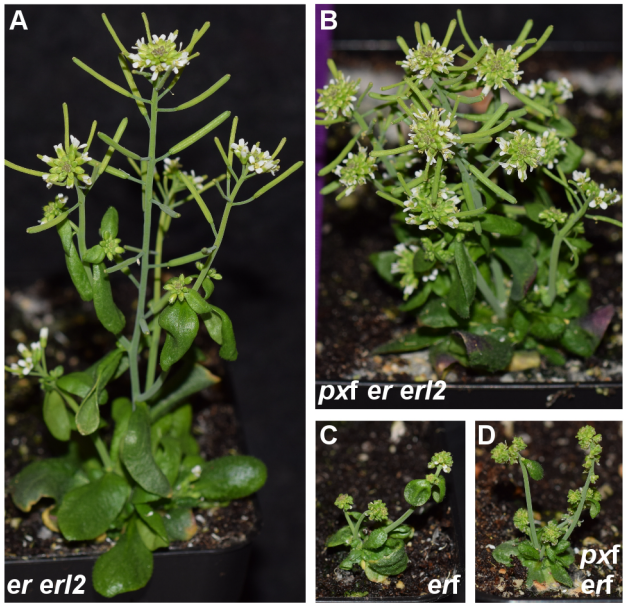

Figure S7. Gross morphology of a subset of mutant lines. (A) *er erl2*. (B) *pxf er erl2*. (C) *erf*. (D) *pxf erf* at 6 weeks old. Images were taken at the same magnification.

Table S1. Vascular proliferation and morphology characteristics of *pxf er* mutant combinations.

Genotype	Vascular bundle size and shape		Hypocotyl diameter (mm)
	cells per bundle	ratio tangential:radial	
Wild type	438.2 ± 15.74	0.61 ± 0.02	1.34 ± 0.04
pxy	347.6 ± 21.79	0.56 ± 0.02	1.24 ± 0.04
er	463.1 ± 23.05	0.67 ± 0.03	1.27 ± 0.05
pxy er	338.2 ± 30.13	1.36 ± 0.18	1.01 ± 0.06
er erl1 erl2	182.3 ± 20.60	0.65 ± 0.06	0.85 ± 0.04
pxy pxl1 pxl2	305.3 ± 38.35	0.91 ± 0.18	1.14 ± 0.04
pxy pxl1 pxl2 er	202.5 ± 28.84	2.30 ± 0.23	0.97 ± 0.06

values are ± S.E.M.

Table S2. *p* values from comparisons of cells per vascular bundle for each genotype tested (ANOVA + LSD).

compared genotypes		*p* value
WT	*er*	0.507
	er pxf	<0.001
	pxy	0.018
	pxy er	0.009
	pxf	0.001
er	WT	0.507
	er pxf	<0.001
	pxy	0.003
	pxy er	0.001
	pxf	<0.001
pxf er	WT	<0.001
	er	<0.001
	pxy	<0.001
	pxy er	0.001
	pxf	0.008
pxy	WT	0.018
	er	0.003
	er pxf	<0.001
	pxy er	0.802
	pxf	0.262
pxy er	WT	0.009
	er	0.001
	er pxf	0.001
	pxy	0.802
	pxf	0.382
pxf	WT	0.001
	er	<0.001
	er pxf	0.008
	pxy	0.262
	pxy er	0.382

Table S3. *p* values from comparisons of hypocotyl diameter for each genotype tested (ANOVA + LSD).

compared genotypes		*p* value
WT	*er*	0.048
	er pxf	<0.001
	pxy	0.028
	pxy er	<0.001
	pxf	0.001
er	WT	0.048
	er pxf	0.001
	pxy	0.816
	pxy er	<0.001
	pxf	0.142
pxf er	WT	<0.001
	er	0.001
	pxy	0.002
	pxy er	0.240
	pxf	0.062
pxy	WT	0.028
	er	0.816
	er pxf	0.002
	pxy er	<0.001
	pxf	0.214
pxy er	WT	<0.001
	er	<0.001
	er pxf	0.002
	pxy	<0.001
	pxf	0.214
pxf	WT	0.001
	er	0.142
	er pxf	0.062
	pxy	0.214
	pxy er	0.003

Table S4. *p* values from comparisons of cell perimeters measured from the vascular cells of each genotype tested (ANOVA + Tukey). Values in grey boxes were not significantly different at the 95% confidence level.

Statistical differences between hypocotyl cell perimeters

Compared genotypes	**xylem**			**phloem**
	vessel	fibres	parenchyma	
WT - *pxf*	0.001	0.007	< 0.0001	< 0.0001
WT - *pxf er*	0.001	< 0.0001	0.014	< 0.0001
WT - *pxf er erl1*	0.515	< 0.0001	1.000	0.374
WT - *pxf er erl2*	0.232	< 0.0001	0.826	0.388
WT - *pxf erf*	0.031	n.d.	0.567	< 0.0001
pxf - *pxf er*	1.000	0.132	< 0.0001	1.000
pxf - *pxf er erl1*	0.192	0.652	< 0.0001	0.001
pxf - *pxf er erl2*	< 0.0001	0.036	< 0.0001	0.001
pxf - *pxf erf*	< 0.0001	n.d.	< 0.0001	0.204
pxf er - *pxf er erl1*	0.193	0.863	0.037	0.001
pxf er - *pxf er erl2*	< 0.0001	0.987	< 0.0001	0.001
pxf er - *pxf erf*	< 0.0001	n.d.	0.579	0.188
pxf er erl1 - *pxf er erl2*	0.001	0.570	0.639	1.000
pxf er erl1 - *pxf erf*	< 0.0001	n.d.	0.769	< 0.0001
pxf er erl2 - *pxf erf*	0.967	n.d.	0.048	< 0.0001

Table S5. *p* values from pairwise comparisons of cell areas calculated from vascular cell types in the hypocotyl (ANOVA + Tukey). Values in grey boxes were not significantly different at the 95% confidence level.

Compared genotypes	vessel	xylem fiber	parenchyma	phloem
WT - *pxf*	0.001	< 0.0001	< 0.0001	< 0.0001
WT - *pxf er*	0.001	< 0.0001	0.051	< 0.0001
WT - *pxf er erl1*	0.068	< 0.0001	0.908	0.632
WT - *pxf er erl2*	0.787	< 0.0001	1.000	0.732
WT - *pxf erf*	0.231	n.d.	0.333	< 0.0001
pxf - *pxf er*	1.000	0.973	< 0.0001	0.922
pxf - *pxf er erl1*	0.819	0.995	< 0.0001	0.001
pxf - *pxf er erl2*	< 0.0001	0.798	< 0.0001	0.001
pxf - *pxf erf*	< 0.0001	n.d.	< 0.0001	0.036
pxf er - *pxf er erl1*	0.833	1.000	0.456	0.033
pxf er - *pxf er erl2*	< 0.0001	0.987	0.034	0.020
pxf er - *pxf erf*	< 0.0001	n.d.	0.963	0.001
pxf er erl1 - *pxf er erl2*	0.001	0.953	0.848	1.000
pxf er erl1 - *pxf erf*	< 0.0001	n.d.	0.922	< 0.0001
pxf er erl2 - *pxf erf*	0.941	n.d.	0.255	< 0.0001

Table S6. Pairwise comparisons of cell perimeters from vascular cells in the inflorescence stem. *p* values were calculated using ANOVA + Tukey. Values in grey boxes were not significantly different at the 95% confidence level.

Genotypes compared	**Xylem**		**phloem**
	vessel	fibres	
WT - *pxf*	0.001	0.136	< 0.0001
WT - *pxf er*	0.004	< 0.0001	0.012
WT - *pxf er erl1*	0.002	< 0.0001	< 0.0001
WT - *pxf er erl2*	< 0.0001	0.996	< 0.0001
WT - *pxf erf*	< 0.0001	n.d.	< 0.0001
pxf - pxf er	0.999	< 0.0001	0.773
pxf - pxf er erl1	1.000	< 0.0001	0.227
pxf - pxf er erl2	0.008	0.055	0.009
pxf - pxf erf	< 0.0001	n.d.	< 0.0001
pxf er - pxf er erl1	1.000	0.528	0.006
pxf er - pxf er erl2	0.002	< 0.0001	< 0.0001
pxf er - pxf erf	< 0.0001	n.d.	< 0.0001
pxf er erl1 - pxf er erl2	0.004	< 0.0001	0.843
pxf er erl1 - pxf erf	< 0.0001	n.d.	0.001
pxf er erl2 - pxf erf	< 0.0001	n.d.	0.058

Table S7. *p* values from pairwise comparisons of vascular cell area from inflorescence stems (ANOVA + Tukey). Values in grey boxes were not significantly different at the 95% confidence level.

Genotypes compared	Xylem		phloem
	vessel	fibres	
WT - *pxf*	0.0004	0.420	<0.0001
WT - *pxf er*	0.0003	<0.0001	<0.0001
WT - *pxf er erl1*	<0.0001	0.001	0.632
WT - *pxf er erl2*	<0.0001	0.855	0.732
WT - *pxf erf*	<0.0001	n.d.	<0.0001
pxf - *pxf er*	0.999	<0.0001	0.922
pxf - *pxf er erl1*	0.993	<0.0001	0.001
pxf - *pxf er erl2*	0.015	0.052	0.0005
pxf - *pxf erf*	<0.0001	n.d.	0.036
pxf er - *pxf er erl1*	0.995	0.021	0.033
pxf er - *pxf er erl2*	0.016	<0.0001	0.020
pxf er - *pxf erf*	<0.0001	n.d.	0.001
pxf er erl1 - *pxf er erl2*	0.076	0.040	0.999
pxf er erl1 - *pxf erf*	<0.0001	n.d.	<0.0001
pxf er erl2 - *pxf erf*	0.001	0.855	<0.0001

Table S8. Primers used in this manuscript

Name	sequence	function
ERL2_F	TGTGGATAACGAGGCCAACT	qRT-PCR
ERL2_R	ATGTGTCCTGAGTCCATGCA	qRT-PCR
ER_F	CACGGCTCACTGAGAAATCC	qRT-PCR
ER_R	TCACTTCATTGTTCCCCGTC	qRT-PCR
ERL1_F	ACTGGGAAGAAAGCAGTGGA	qRT-PCR
ERL1_R	CCTCTGGATCAACTGCTTCC	qRT-PCR
EPFL4_F	CTTCTCCGCCTCCTCCATAG	qRT-PCR
EPFL4_R	ACTCCTTATGAACCCACCCG	qRT-PCR
EPFL5_F	GTCCTCCCAACTCTCATCGT	qRT-PCR
EPFL5_R	ACCCGACCTAGCTATCTCCT	qRT-PCR
EPFL6_F	AGAAATTCTCAGCCGTCGGA	qRT-PCR
EPFL6_R	ACGGTACTCTTGCCTTCCTC	qRT-PCR
PXY_F	AGCATGGGTAGGTCGTGTAG	qRT-PCR
PXY_R	CAACACATCTCTCATCGGCG	qRT-PCR
PXL1_F	GACGTGGTTGAGTGGATTCG	qRT-PCR
PXL1_R	GGTGCAGAGAAGAGCGATTC	qRT-PCR
PXL2_F	AACGGAAACCTTGGTGATGC	qRT-PCR
PXL2_R	TCATGGTGGAGGTAAGCGAG	qRT-PCR
qRT_18s_rRNAf	CATCAGCTCGCGTTGACTAC	qRT-PCR
qRT_18s rRNAr	GATCCTTCCGCAGGTTCAC	qRT-PCR
qACT2f	GCCATCCAAGCTGTTCTCTC	qRT-PCR
qACT2r	ACCCTCGTAGATTGGCACAG	qRT-PCR
JL202 LB	CATTTTATAATAACGCTGCGGACATCTAC	genotyping
ERL1_LP	TTCATGTGCAGCCTTGAATC	genotyping
ERL1_RP	GCAATTGGCCAAGTTCAGTT	genotyping
ERL2_LP	TTCCCATGAACATTGCTGAA	genotyping
ERL2_RP	CCGGAAGTGATTGGTCTGAT	genotyping
ER-1	tttgtttttgtgcgtgtgtg	genotyping
ER-2	ATCATTCGGCTGTCTTTTGG	genotyping
GABI-LB	ATATTGACCATCATACTCATTGC	genotyping
pxl2-1(salk)F	ACCTCTATGCCACACACCAAG	genotyping
pxl2-1(salk)R	CAAGCTCTGACGGAATCTCAC	genotyping
salk_LBa1	TGGTTCACGTAGTGGGCCATCG	genotyping
pxl1-1(salk)F	AATCGATGGTCTATCCTTCGG	genotyping
pxl1-1(salk)R	TATGCGGTGGAGTTCTACCAC	genotyping
ER-GUSF	accactgtaaatttccgccag	genotyping
ER-GUSR	aagacttcgcgctgatacca	genotyping
ERL1-GUSF	acgccgttacttatctccgt	genotyping
ERL1-GUSR	atccagactgaatgcccaca	genotyping
ERL2-GUSF	tagaaccgtcgccgtcaaat	genotyping
ERL2-GUSR	ttcacgggttggggtttcta	genotyping
ERL1 DT1-BsF	ATATATGGTCTCGATTGCCAATTGCAGAGACTTGCAGTT	erl1-GE clone
ERL1 DT1-F0	TGCCAATTGCAGAGACTTGCAGTTTTAGAGCTAGAAATAGC	erl1-GE clone
ERL1 DT2-R0	AACTTAGATGATTGCCAGCAAGCAATCTCTTAGTCGACTCTAC	erl1-GE clone
ERL1 DT2-BsR	ATTATTGGTCTCGAAACTTAGATGATTGCCAGCAAGCAA	erl1-GE clone
VErl1_F	GAATTTGTCCAGTCTGAATCTTGG	erl1-GE genotyping
VErl1_R	CAAGTACCACAAACCGGTTAGC	erl1-GE genotyping